First-In-Flight Full-Scale Application of Active Flow Control: The XV-15 Tiltrotor Download Reduction

Prof. Hassan M. Nagib and Dr. John W. Kiedaisch
Illinois Institute of Technology
MMAE Department
10 W. 32nd St.
Chicago, IL 60616
U.S.A.

E-mail: nagib@iit.edu / kiedaisch@iit.edu

Prof. Israel J. Wygnanski and Aaron D. Stalker
University of Arizona
AME Department
1130 N. Mountain
Tucson, AZ 85721
U.S.A.

E-mail: wygy@ame.arizona.edu / astalker@email.arizona.edu

Tom Wood
Bell Helicopter Textron
600 E. Hurst Blvd.
Hurst, TX 76053
U.S.A.

E-mail: TWood@bellhelicopter.textron.com

Michael A. McVeigh
Boeing Helicopters
P.O. Box 16858
Philadelphia, PA 19142
U.S.A.

E-mail: michael.a.mcveigh@boeing.com

REPORT DOCUMENTATION PAGE

Form Approved
OMB No. 0704-0188

1. REPORT DATE *(DD-MM-YYYY)*	2. REPORT TYPE	3. DATES COVERED *(From - To)*
October 18, 2004	Final	22 November 2003 to 21 December 2003

4. TITLE AND SUBTITLE
First-In-Flight Full-Scale Applications of Active Flow Control: The XV-15 Tiltrotor Download Reduction

5a. CONTRACT NUMBER
W911NF-04-1-0012

5b. GRANT NUMBER

5c. PROGRAM ELEMENT NUMBER

6. AUTHOR(S)
Hassan M. Nagib and John W. Kiedaisch

5d. PROJECT NUMBER

5e. TASK NUMBER

5f. WORK UNIT NUMBER

7. PERFORMING ORGANIZATION NAME(S) AND ADDRESS(ES)
Illinois Institute of Techonology
3300 S. Federal Street
Chicago, IL 60616-3793

8. PERFORMING ORGANIZATION REPORT NUMBER

9. SPONSORING/MONITORING AGENCY NAME(S) AND ADDRESS(ES)
US Army Robert Morris Acq Ctr - W911NF
Research Triangle Park Contracting
AttN; AMSSB-ACC-R
P. O. Box 12211
Research Traingle Park, NC 27709-2211

10. SPONSOR/MONITOR'S ACRONYM(S)

11. SPONSOR/MONITOR'S REPORT NUMBER(S)
45829.1-EG

12. DISTRIBUTION/AVAILABILITY STATEMENT

Approved for Public Release; Unlimited Availability

13. SUPPLEMENTARY NOTES

14. ABSTRACT

See attached

15. SUBJECT TERMS

16. SECURITY CLASSIFICATION OF:			17. LIMITATION OF ABSTRACT	18. NUMBER OF PAGES	19a. NAME OF RESPONSIBLE PERSON
a. REPORT	b. ABSTRACT	c. THIS PAGE		29	Hassan M. Nagib
					19b. TELEPHONE NUMBER *(Include area code)* 312-567-3010

ABSTRACT

In June 2003, before being retired to the Smithsonian Museum Annex, near Dulles Airport, the only remaining XV-15 tiltrotor aircraft was used for a series of flight tests to demonstrate the effectiveness of Active Flow Control (AFC) in reducing the download during hover. The flaps/ailerons were retrofitted with actuators delivering zero-mass-flux periodic jets emanating from slots positioned tangential to the surface. The flight tests followed two extensive sets of model experiments, and the program included participation from University of Arizona, Illinois Institute of Technology, Tel Aviv University, Bell Helicopter and Boeing under the sponsorship of the Micro-Adaptive Flow Control (MAFC) program of DARPA. The over six hours of flight tests successfully achieved the two goals and documented reduction in the download forces by 9 to 14 %, thereby demonstrating for the first time that the aerodynamic principals of AFC extend to full-scale flight.

This successful application of AFC opens new vistas in the design of products using novel fluid dynamic concepts. It may not only generate new configurations of airplanes or combustors but it may also be used in many medical and biological applications; after all, most of the flows in humans and animals are pulsating and often separated. This requires an infrastructure that considers unsteady flow parameters with the same commitment as the infrastructure that was built nearly half a century ago to understand high-speed flows. Furthermore the development of actuators from micro to macro size will need to be addressed, if active flow control is to truly succeed in a ubiquitous way. The experience gained from the XV-15 download reduction will be discussed with an emphasis on new insight and physical understanding in the context of this broadly defined flow control of separation.

1.0 NOMENCLATURE

α wing angle of attack, degrees

A disc area of two rotors, sq. m

AFC Active Flow Control

c wing chord, flaps up, m

c_f flap chord, m

C_μ momentum coefficient, $(h/c)(U_j / U_\infty)^2$

C_d section drag coefficient, drag/$(0.5\ \rho\ U_\infty^2\ c)$

C_l section lift coefficient, lift / $(0.5\ \rho\ U_\infty^2\ c)$

C_W aircraft weight coefficient, weight / $(\rho\ A\ V_T^2)$

c_p pressure coefficient, Δp / $(0.5\ \rho\ U_\infty^2)$

C_P rotor power coefficient, 550 total RHP / $(\rho\ A\ V_T^3)$

C_T rotor thrust coefficient, total thrust / $(\rho\ A\ V_T^2)$

δ_f flap deflection angle, degrees

DL wing download, N

f blowing frequency, Hz

F^+ non-dimensional frequency, $f\, x_{te} / U_\infty$

h slot width, m

ρ air density, kg/m^3

T total rotor thrust, N

U_∞ remote wind speed, m/s

U_j peak jet exit velocity, m/s

V_T rotor tip speed, m/s

W aircraft weight, N

x chordwise distance, m

x_{te} distance from AFC slot to trailing edge, m

2.0 INTRODUCTION

2.1 Background and Motivation

A research program funded by DARPA, under the Micro-Adaptive Flow Control program (MAFC), has recently culminated in a successful full-scale flight demonstration on the XV-15 experimental airplane, shown in Figure 1, using a novel concept that reduces the air resistance, or drag, during takeoff and hover. The tests were conducted at the Bell Helicopter flight center in Arlington, TX, in collaboration with researchers from the University of Arizona, the Illinois Institute of Technology, and the Boeing Company.

Nearly all aerodynamic and hydrodynamic applications exhibit regions where the flow is not able to follow the local contour of the body, and therefore "separates" from it. In various transportation vehicles, ranging from airplanes to ships, trains, trucks, and automobiles, these "separated" parts of the flow are responsible for losses that often lead to increased fuel consumption, limitation on travel range or speed, and in the carrying capacity of the vehicle. These losses are often reflected in the lift and drag forces. In airplanes that take off vertically like a helicopter and then change their configuration to fly as a normal airplane, e.g., "tilt-rotor airplanes" like the V-22 "Osprey," these losses are most evident in resistance to the upward motion of the horizontal wing through the air during takeoff. The resulting resistance is called "download" and its reduction would have a major impact on the carrying capacity and operational range of such vehicles.

For a long time, engineers have tried various means of manipulating the flow so as to prevent it from separating. Some of these techniques were eventually used on military airplanes, and involved the steady blowing or suction of air out of orifices located in or near the separated flow region. For nearly two decades, scientists and engineers have conducted laboratory tests, often in wind tunnels, to investigate a novel idea of using periodically pulsating small jets emanating from slots in the surface to prevent separation of the flow. This approach has the potential of higher efficiency and is often referred to as Active Flow Control (AFC). These recent developments are based on the understanding that the previously believed random nature of the turbulent flows near and around bodies contains and is influenced by regular or semi-periodic large scale motions. Therefore, periodic perturbations may be used to alter the steady characteristics of the flow. The initial ideas that germinated in university laboratories were generally discounted by industry because of the lack of their full-scale demonstration.

The roots for the research culminating in the recent successful flight tests developed after Dr. J. McCroskey of NASA-Ames Research Center visited the Aero-Lab at Tel-Aviv University where he had observed a demonstration of stall-delay on a wing section by a periodic pulsation of a jet emanating from a narrow slot. He suggested testing the technique on the flapped wing of a tiltrotor aircraft in hover because of the large wing download encountered in this flight regime. The concept was immediately tested at the university and success of these tests enabled Dr. Wygnanski to contract with the Boeing Company and DARPA for an extensive investigation using scaled models of tilt-rotor airplanes at the University of Arizona.

The applications of AFC open new vistas in the design of transportation vehicles of all types, and many other products associated with fluid flow. These new directions may not only generate new configurations of airplanes or combustors but may also be used in many medical and biological applications; after all, most of the flows in humans and animals are pulsating. This requires an infrastructure that considers unsteady flow parameters with the same commitment as the infrastructure built for the exploration of high-speed flows. Furthermore, the development of actuators from micro to macro sizes has to be addressed, if active flow control is to succeed.

2.2 Objectives

All aircraft utilizing tiltrotor configurations experience a download in hover caused by drag induced from the rotor downwash acting on the wing and fuselage. This download represents a significant penalty in payload or vertical lift capability. Current design practice is to deflect the full-span wing flaperons to high angles (~ 60 to 70 degrees) to reduce the area exposed to the rotor downwash. This reduces the download to about 10% of thrust. When the flaps are deflected to angles greater than these, the flow separates from the shoulder of the flap and the download increases. Various attempts to further reduce the download using mechanical devices have been reported and, while some of these have demonstrated appreciable reductions in download, none has yet been implemented in a production design. In two recent papers, Darabi et al. [1] and McVeigh et al. [2] describe the extensive first phase of the model tests and some highlights of the flight demonstration of the XV-15. The main purpose of the present paper is to bring to the attention of the community some other aspects of the investigation that were vital in achieving a successful test flight. In particular, here we will tell the story about the development of the actuators, the simulation of the flow around the flap in its full size, and the determination that the actuators can indeed operate under the pressure differential that exists between the upper and lower surface. In this second phase of the model tests, all the details of the airplane are simulated, but not necessarily the fluid dynamics associated with the wing.

3.0 LABORATORY TESTS

3.1 Actuator Development

The actuators used in the XV-15 powered-model tests at the University of Arizona (U of A) were developed by Nagib and Associates at the Illinois Institute of Technology (IIT). This generation of actuators is called ATEAM-9, where "ATEAM" stands for Aerodynamically and Thermally Engineered Actuator Modules. These actuators are voice-coil based actuator modules designed to deliver high peak-jet velocities over a wide frequency range without the need for cooling. The square frames are designed to fit together in a linear array beneath specifically designed slotted cover plates. The top surfaces of the actuator frames are designed to seal against the lower surface of the cover plate. For the tests at U of A, there was insufficient room in the model flaps to install these actuators directly in the flap, so they were mounted in the main element of the wing and ducts were used to channel the forcing to the slots in the flaps [1] [3].

High temperature materials and adhesives were utilized in the construction of the actuators. The circular voice coil consists of two layers of copper magnet wire wound on a polyimide substrate (called the former). The former material extending up from the winding to the piston is reinforced with a Nomex® collar. The piston consists of a sheet of flexible material that is clamped in the actuator frame. Bonded to the center of the flexible sheet is a rigid composite piston which provides a stable surface to which the coil is also bonded. The steel armature contains a radially magnetized rare-earth magnet ring. The armature design was optimized using magneto-static Finite Element Modeling (FEM) to achieve the strongest magnetic field in the coil gap, while staying within the size limitations dictated by the model design. The aluminum actuator frame was designed for optimal heat transfer from the armature to the surrounding material using thermal FEM. With this design, an actuator cooling system was not required.

3.2 2-D Wind Tunnel Tests and 3-D Powered Model Tests

An extensive data base was developed at the University of Arizona by Professor Wygnanski and his group over a number of years starting with 2-D airfoil tests and culminating with a full powered model of the XV-15. The details of these experiments have already been published [1] [3]. The two dimensional airfoils varied in scale but were generally tested in open return wind tunnels with a test section having two open sides to minimize the blockage. Most of the basic AFC results were developed on such models while varying a number of parameters like AFC amplitude and frequency, slot location and orientation, and flap deflection angle. A 16.67% scale model of the XV-15 was specially constructed for this phase of testing. The model incorporates five main components including a fuselage with tail, a wing (hollow to allow installation of actuators), adjustable flaps, nacelles, and rotors. The tilt-rotor model was suspended from an A-frame structure in an inverted arrangement, thus guiding the rotor downwash up toward the ceiling, which is more than five rotor diameters away. The rotors were not coupled to the nacelles to allow for a direct measurement of the aerodynamic forces on the model. In general, the experiments were run at selected values of rotor RPM, and a fixed collective pitch, making the thrust a function of RPM. Initially, the thrust values were evaluated from wake velocity measurements, using a Kiel probe, with no model present. Later in the program two six component balances were supplied by Boeing and installed below the rotor hub and two torque transducers were also installed to directly measure the power requirements of the rotors.

4.0 XV-15 AFC SYSTEM DESIGN

In order to implement AFC on the XV-15 aircraft, new, special-purpose flaps and ailerons were designed and built by Bell Helicopter. Also, new AFC actuators were designed and built by Nagib and Associates at IIT. The flaps and actuators were designed to work together as a system; the actuator size was defined by the available space in the flap and by the slot location, the internal structure of the flaps was modified to accommodate the largest actuator possible, and the slot design was optimized to work specifically with the new actuators. The resulting system is shown in Figure 2. The actuators were installed in bays, with a total of 10 actuators in each flap and 16 actuators in each aileron. The slot was located at 10% of the flap chord and the slot width was nominally 0.045 inches (1.1 mm). The slot was integrated into a removable cover plate that sealed against the top of the linear array of actuators in each bay. This allowed easy access to the actuators for inspection and replacement, as needed. The new flaps and ailerons were actuated to move together to the same deflection angle and were qualified for hover and very low speed flight only.

The actuators developed for the XV-15 flight tests, designated ATEAM-15 actuators, are of the same basic design as the ATEAM-9 actuators used for the U of A powered model tests; however they are larger and more powerful. A single actuator is shown in Figure 3. The internal actuator components, the coil, magnet, armature, and piston, were optimized to give the required forcing amplitude (60 – 100 m/s peak velocity at the slot exit) over the desired frequency range (50 – 100 Hz). As with the ATEAM-9, extensive finite element modeling was used to optimize the design of the magnet, armature, and actuator frame. The actuators were hand assembled and individually tested for quality and consistency. Figure 4 shows the single-actuator test fixture that was used. This fixture accommodates different slotted cover plates that allowed the slot design to be optimized. Throughout this process, detailed calibrations were conducted using a hot-wire probe to measure the fluctuating velocity at the slot exit, as shown in Figure 5. Additional details of the actuator design can be found in reference [2].

To power the AFC actuators on the aircraft, two commercial professional-grade audio amplifiers were used. One amplifier was used to drive the entire set of 26 actuators on each wing. A wiring study was performed to determine the optimal wiring arrangement for the actuators. The chosen wiring configuration gave the optimum distribution of available power across the span of the wing.

5.0 PRE-FLIGHT ACTUATOR INTEGRATION

5.1 Full-Scale Flap Model Wind Tunnel Tests

In order to ensure smooth integration of the actuators into the aircraft and verify the actuator performance under simulated flight conditions, experiments were performed using a full-scale model of the XV-15 AFC flap section. This turned out to be a very important step for transitioning from laboratory experiments to the full-scale flight test.

5.1.1 Flap Model Design

A full-scale model of a two-dimensional section of the XV-15 flap, complete with AFC slot, was fabricated and tested in the high-speed test section of the National Diagnostic Facility (NDF) wind tunnel at IIT at the expected flight conditions. The model was designed to hold up to five ATEAM-15 actuators. Figure 6 shows an illustration of the model in the wind tunnel test section and, for comparison, a drawing of the full XV-15 wing section. Because of the size of the test section (0.61 m high by 1.52 m wide), the flap model was installed with a truncated main wing element that was designed to give separated flow conditions over the flap

that were similar to those seen in the powered-model tests at the University of Arizona [3]. It is important to recognize that the download on the XV-15 is mostly due to the main element, which represents 70% of the chord of the airfoil; i.e., the base pressure over that large area compared to the 30% chord flap. In the case of the model in the NDF, the "full-size" flap represents 57% of the chord and the streamlines impinging on the upper surface are excessively deflected and move outside of the test section walls. However, it should be stressed that the main purpose of the model-flap tests was to qualify the actuators and their operating parameters under a representative environment similar to the XV-15 airplane. Therefore, what was most important was not the detailed distribution of the pressure over the flap, but for example, the pressure differential that is experienced by the actuators, the effective cooling of the actuators, their possible interaction, etc. We deemed these tests, with a full-scale model flap and actuator system, an essential step on the way to the flight demonstration; although we did not expect that all the fluid dynamics details would be exactly replicated.

The flap model was designed to have all the key features of the actual XV-15 AFC flaps, and its construction closely resembled the construction of the actual flaps. Some of the leading edge features of the XV-15 AFC flaps are shown in Figure 7. There are cutouts in the leading edge for the aileron drive links to pass through. These are open to the slipstream during hover. The flap model was designed to have a similar cutout at one end of the model. Some details of the flap model design are shown in Figure 8, including the interior of the leading edge, the cove between the main element and the flap, and the cove cover on the upper surface of the main element at the trailing edge. The interior of the flap model was designed to closely simulate the interior of the actual flaps. The actuator position was identical to the position of the actuators in the actual XV-15 flaps. The drive shaft, which is in close proximity to the bottom of the actuators, was also included in the flap-model design. The location, contour, width, and exit angle of the AFC slot on the flap model were identical to the slot design used on the aircraft.

The actuator power wiring and connectors used in the flap model were identical to those used on the aircraft. This allowed us to troubleshoot any problems with the wiring configuration and make preliminary impedance measurements that would allow us to estimate the actuator power consumption. The flap and main element were instrumented with a total of 24 pressure taps at the center-span location. An additional pressure tap was installed inside the flap leading edge in the area beneath the actuators. The actuator wiring and pressure tubing exited the flap through a cutout on the lower flap surface, similar to the way the power cables exit the actual XV-15 AFC flaps.

Figure 9 shows the flap model and truncated main element installed in the NDF test section. The model was mounted between two circular mounting plates. The mounting plates rested in large bearings that allowed the angle of attack to be changed. Tufts were placed on the upper flap surface for flow visualization. Also seen in Figure 9 are the leading edge cutout described earlier and the roughness that was added during the tests to trip the boundary layer on the main element. The reason for this will be described later.

5.1.2 CFD Analysis of Full-Scale Flap Model

Prior to conducting the wind tunnel tests, a series of computations were conducted at the University of Arizona to investigate the blockage effects in the wind tunnel and to make a preliminary comparison between the flow field over the flap model in the wind tunnel and the flow field over the full XV-15 wing. The computations were performed using a semi-implicit, fractional step finite element method (FEM) with a large eddy simulation (LES) turbulence model [4] [5] [6]. The grid used is shown in Figure 10. The grid extends far upstream and downstream of the model and has solid boundaries on both sides. Computed pressure coefficient distributions over the flap model are in Figure 11. Figure 11a shows the baseline case with no AFC, and

Figure 11b shows a typical case with AFC applied. For comparison, Figure 12 shows both computed and experimental pressure coefficient distributions over the XV-15 wing from reference [6]. Figure 12a shows the baseline case and Figure 12b shows the case with AFC. Figures 13 and 14 compare the wakes of the flap model without AFC (13a) and with AFC (13b) to the wakes of the XV-15 wing without AFC (14a) and with AFC (14b) [6]. The instantaneous pressure contours shown in these figures illustrate how the application of AFC at the flap shoulder eliminates the large-scale recirculation in the wake and attaches the flow on the flap, resulting in a reduction in download. Figure 15 shows a close-up view of the time-averaged velocity vectors over the flap (baseline case in Figure 15a, AFC case in Figure 15b). This figure clearly shows a reduction in the size of the separated region with AFC applied. For all these comparisons, the computed flow field over the flap model in the NDF is qualitatively similar to the flow over the XV-15 wing. Therefore, the flap model tests provided an adequate representation of the download characteristics and AFC effects expected on the XV-15 under flight conditions.

5.1.3 Flap Model Test Configurations

Due to the many detailed features of the XV-15 AFC flaps and, consequently, the flap model, a number of different configurations were run during the wind tunnel tests. The model configuration was varied in order to reveal the effects of modifying certain features and to determine the configuration that was most representative of the expected flight conditions.

The blockage effects were investigated by opening either the front door, back door, or both doors of the test section in the area adjacent to the model (shown schematically in Figure 6). It was found that the best tunnel configuration was to have the back door closed and the front door open. (The view in Figure 9 is the view through the open front door of the test section.) Because of the low Reynolds numbers at which these tests were run, roughness was added to the stagnation region of the main element. This was found to give results that were more comparable to the powered model tests performed at the U of A and thus to the expected behavior of the XV-15 during flight. The dependence of the separated region on the state of the separating shear layer is often very complex. In particular, depending on whether the separating layer is laminar, transitional or fully turbulent, the separated region may display substantially different characteristics.

Different model configurations were achieved by opening/sealing the leading edge cutout, opening/sealing the cable exit hole, installing/removing the cove cover, and opening/sealing/partially sealing the cove between the main element and the flap. Various combinations of these variations were tested. For these different configurations, data was taken at a number of different angles of attack ranging from -90 deg. to -50 deg. Once the most representative configuration was found, a number of runs were conducted with AFC at frequencies ranging from 30 to 120 Hz and at a number of forcing amplitudes.

One final configuration change was made towards the end of these tests. Since a leading-edge Kruger flap was planned to be installed on the XV-15 for a portion of the flight tests, a similar Kruger flap was added to the leading edge of the wind tunnel model. A limited number of runs were performed in this configuration.

5.1.4 Flap Model Wind Tunnel Test Results

As expected, varying the model angle of attack significantly effected the pressure distribution. Examples of these changes are illustrated in Figures 16 and 17. These figures show the pressure-coefficient distribution over the model for four different flap deflections; 45, 55, 65, and 75 degrees. We should emphasize again that due to the shortened main element of the model, and the high tunnel blockage, the stagnation region pressure coefficients are highly exaggerated; since they are normalized by the upstream velocity in the tunnel. It was

shown in the powered model tests at the U of A and in previous XV-15 flight tests that during hover, the flow over the flap separates and the flap stalls at deflection angles near 60 or 65 degrees. For the flap model, at an angle of attack of -90 degrees (Figure 16), the flap is not stalled even at deflections up to 75 degrees. By changing the angle of attack to -50 degrees (Figure 17), the flap stalls at a deflection somewhere between 55 and 65 degrees. The runs shown in these figures were performed with the roughness added to the stagnation region on the main element. Figure 18 shows the pressure distributions at an angle of attack of -50 degrees for runs without the added roughness. Comparing Figures 17 and 18, the effect of tripping the boundary layer on the main element can be clearly seen. Without the added roughness, the flow over the flap is still attached at a deflection of 65 degrees and is only beginning to stall at a deflection of 75 degrees. Therefore in order to simulate the separation characteristics of the powered model tests at the U of A and the expected flight conditions using this flap model, it is necessary to trip the boundary layer on the main element and run at an angle of attack near -50 degrees. Through further testing, it was found that an angle of attack of -60 degrees gave the closest comparison to the U of A tests.

It is clear also from comparing Figures 17 and 18 that the condition of the separated shear layer can be of great impact on the subsequent behavior of separation. While it is very difficult to understand the interaction and coupling between phenomena such as shear-layer transition, local flow curvature, entrainment and mixing, circulation and vorticity within the separated flow, and trailing edge (or Kutta like) conditions, it is important to represent the upstream flow conditions as faithfully as possible in model experiments. While the unsteady and vortical flow generated by the rotors was virtually impossible to replicate in the model-flap experiments in the NDF (although they were considered at one point), we at least strived to represent the high level of turbulence in the separating shear layer.

One of the most important quantities that needed to be measured was the pressure difference across the AFC actuators. The AFC slot location is at the shoulder of the flap, and a substantial suction pressure can exist in this region under certain flow conditions. Since there is no way to control the pressure in the flap interior beneath the actuators, a substantial pressure difference can exist between the slot-side of the actuator piston and the flap interior. Such a pressure difference changes the static position of the actuator piston. If the piston position is significantly changed, the range of motion is limited and, therefore, the maximum excitation amplitude (U_j) is diminished. In order to design the actuators for optimum performance under flight conditions, it was necessary to have an accurate estimate of the expected pressure difference under flight conditions. Figure 19 shows how the pressure difference across the actuators measured on the flap model at a free-stream velocity of 30 m/s varies with flap deflection angle. Four different angles of attack are shown. This figure demonstrates that for the range of flap deflections expected during the flight tests, pressure differences of a magnitude slightly higher than 0.4 psi (2.8 kPa) can be reached. This data was crucial to the actuator development effort, and because of it, modifications to the actuator design were made that will be discussed later. The curve in Figure 19 corresponding to an angle of attack of -60 degrees should be noted. This curve will be compared to pressure difference measurements made during the flight tests later in this paper. It is important to also recognize that the model tests are not completely representative because of the interaction between the angle of attack and the gap between the airfoil main element and the flap as discussed next.

The gap in the cove, between the main element and the flap, was not originally sealed on the XV-15 aircraft. However, on the powered model used at the U of A, the gap was sealed because of the channels which transmitted the AFC excitation from the actuators in the main element to the slots in the flap [1] [3]. In order to determine the proper configuration for the best AFC performance, test runs were conducted on the flap model to examine the effects of sealing the cove. These results are summarized in Figure 20, which shows the percent change in the base pressure on the flap model, referenced to the base pressure at 75 degrees flap

deflection, with varying flap deflection. The base pressure is used as an indication of the download. Curves are shown for two angles of attack, -50 degrees and -90 degrees, for cases with the cove open, 80% sealed, and 100% sealed. The effect of sealing the cove was determined to be significant enough to warrant implementing a cove seal on the XV-15 aircraft for the flight tests. This configuration was expected to give the best comparison to the U of A powered model test results. Similar tests were run to examine the effects of plugging the leading-edge cutout, removing the cove cover, and sealing the cable exit hole. Based on the results of these tests, it was decided to leave the cove cover in place, leave the leading-edge cutouts open, and leave the cable exit hole open on the XV-15 wing for the flight tests.

Figure 21 shows the baseline pressure coefficient distributions over the flap model for an angle of attack of -60 degrees with the cove sealed. This case gave the best comparison to the U of A powered-model data. Curves are included for flap deflections from 45 to 75 degrees. The flow over the flap remains attached at deflections up to 60 or 65 degrees. Beyond these angles, the flap stalls. Figure 21 shows pressure distributions for the same configuration with AFC applied to the flap. All curves in this figure are for a flap deflection of 70 degrees, which was stalled with no AFC. The results for five different AFC forcing amplitudes are shown at one forcing frequency, 90 Hz. With AFC, the suction peak on the flap is significantly increased, indicating the flow is being re-attached by the AFC. The effects increase with increasing forcing amplitude up to a point (the 73V amplitude in this case), after which no additional benefit of increased amplitude is realized. This same behavior was revealed in the U of A powered model tests [2] [3]. The effect of AFC forcing amplitude on the base pressure (and thus, the download) is shown in Figure 23, which plots the percent reduction in flap model base pressure versus AFC amplitude. Here, the amplitude is represented by the velocity ratio U_j/U_∞, which is the ratio of peak instantaneous AFC jet velocity to the free-stream velocity. There is a moderate reduction in the base pressure coefficient (i.e. increase in the base pressure) at a flap deflection of 65 degrees, which is just past stall in the baseline case, for U_j/U_∞ =3. At 70 degrees flap deflection, there is a substantial decrease in the base c_p once U_j/U_∞ exceeds 3. For both these cases, the AFC effect saturates and no significant reduction in the base c_p is achieved at higher AFC amplitudes. At 75 degrees flap deflection, the base c_p reduction increases as AFC amplitude increases, and no saturation is seen for the range of amplitudes used for these tests. It is likely that the base c_p would continue to be reduced and the AFC effects would eventually saturate at this flap angle if greater AFC amplitudes were available. Figure 24 summarizes the AFC effect by examining the base pressure coefficient plotted versus flap deflection for the baseline (no AFC) case and for the case with AFC applied at an amplitude of 73V, which corresponds to U_j/U_∞ = 4. These results are very similar to the download reduction data from the U of A powered model tests [1] [2] [3]. The effects of AFC forcing frequency were also examined. Figure 25 shows the percent reduction in flap model base pressure coefficient with AFC forcing frequency for different flap deflections. It was found that the greatest reduction in base c_p (download) was achieved with frequencies in the range of 40 to 80 Hz.

In summary, the full-scale flap model tests proved to be an essential step in the process of taking laboratory-proven AFC technology to full-scale flight tests. This test allowed performance optimization of the actuator arrays and estimation of the power requirements. In addition, it allowed the operational parameters, such as amplitude and frequency, to be optimized under realistic flow conditions. The in-flight operating environment inside the flaps was simulated and the thermal operating limits of the actuators were determined. The results of the tests compared well qualitatively with the powered model results, but without the powered-model tests one could have been misguided.

5.2 Actuator Installation and Calibration

5.2.1 Final Actuator Modification

During the full-scale flap model tests described in the previous section, the pressure difference across the actuator pistons was determined under realistic conditions. With this information, additional bench-top actuator tests were conducted to determine the actuator operating limits (maximum amplitude for each frequency) for different pressure differentials. The test fixture shown in Figure 4 was modified to allow the area beneath the actuator to be pressurized, and the piston travel at different operating amplitudes was measured using a "feeler" wire through a hole in the slot cover plate. As a result of these measurements, modifications were made to the actuator piston to allow it to operate under the expected pressure differential. Figure 26 shows a plot of piston deflection versus applied back pressure (equivalent to pressure differential across the actuator) for three different piston designs. The curve labeled Design 1 was the original piston design. After modifications, the final design, Design 3, allowed operation under significantly more pressure differential for the same piston deflection with only a slight drop in peak performance. The small sacrifice in performance was determined to be acceptable in order to improve actuator reliability during the flight tests.

5.2.2 Bench-Top Calibrations

The actuators were installed in the flaps of the XV-15 prior to the installation of the flaps on the aircraft. Figure 27 shows one actuator bay in one of the new XV-15 flaps with the slotted cover plate removed to expose the array of AFC actuators. An installed cover plate is shown in the neighboring bay, to the right in the photo. A detailed series of bench-top calibrations were performed to confirm the performance of the actuators, to document the total impedance (for power requirement calculations), and to test the wiring configuration. The MAFC controller developed by Bell Helicopter for the aircraft, which was later installed in the cockpit, was used to control the actuator frequency and amplitude during these bench-top tests. Also, the amplifiers that were to be used for the flight tests were used during these calibrations. Calibrations of the XV-15 flaps, both on the bench and later on the aircraft, were made using a calibration fixture designed to hold a hot-wire probe and a total-pressure tube side-by-side. This fixture, shown in use in Figure 28, is adjustable to allow the probes to be placed at different spanwise locations along the slots. The hot-wire probe and total-pressure tube were used simultaneously during the bench-top calibrations, and a correlation was developed between the peak slot exit velocity measured with the hot-wire probe and the mean slot exit velocity measured with the total-pressure tube.

An example time trace of the measured slot exit velocity is shown in Figure 29. The hotwire signal is a rectified sine wave with peaks for both the blowing and suction phases of the AFC actuator cycle. Due to the positioning of the hot-wire probe, the blowing peak is higher in amplitude than the suction peak. The data at two different probe positions are shown in this figure corresponding to distances of 0.35 and 0.65 slot widths from the slot exit. For this range of distances from the exit, the magnitude of the blowing peak is relatively constant, while the magnitude of the suction peak drops significantly, therefore the blowing peak can be measured very consistently as long as the probe position is within this range. For these calibrations, the blowing peak (the instantaneous peak jet velocity, U_j), is the quantity used to characterize the actuator performance. The two horizontal lines shown in Figure 29 are the mean slot exit velocities measured with the total-pressure tube. This measurement is more sensitive to probe distance from the slot exit, and therefore care was taken to insure consistent total-pressure tube positioning in subsequent calibrations.

Sample results of the XV-15 AFC system performance are shown in Figure 30. Here, peak slot exit velocity is plotted versus actuation frequency for different amplitudes. The bench-top calibrations documented the

performance of the actuators for different settings of the MAFC controller. They also documented the spanwise variation in forcing amplitude, the effects of varying slot widths, the effects of leakage around the actuator frames, and the effects of varying the venting of the flap interior. During these calibrations, it was found that performance suffered due to leakage between the actuator frames. Simply applying tape to the actuator frames to seal any small gaps resulted in a significant increase in performance, on the order of 7 to 10%. This is illustrated in Figure 30, where the 80 Vrms amplitude data (orange line with solid diamond symbols) is repeated with the tape seal in place (orange line with open circle symbols). The results of these calibrations allowed the operating parameters of the actuators for the flight tests to be finalized. Figure 31 depicts how the MAFC Controller amplitude setting (selected by the pilots during the flight tests) relates to peak slot exit velocity at the two frequencies chosen for the flight tests, 50 and 80 Hz. Different maximum amplitudes were specified that were dependent on the pressure differential across the actuators measured during flight. This served as the basis for developing the flight test plan.

5.2.3 Actuator Installation and Health Monitoring

The bench-top calibrations described in the previous section also allowed the actuator health monitoring systems to be tested. The health monitoring system consisted of thermocouples for measuring actuator temperature and dynamic pressure measurements inside the actuator bays in the flaps. The dynamic pressure measurements were made with fast-responding differential transducers and served two purposes; the mean gave a measurement of the pressure difference across the actuators and the peak-to-peak amplitude of the pressure signal was used to detect an actuator failure, which would result in a decrease in this quantity.

6.0 XV-15 FLIGHT TESTS

6.1 Procedures

The flight testing took place at Bell's Arlington, Texas, flight test facility. Details of the flight test procedures have been described in references [2] and [3] and will not be repeated here. Runs were conducted both with and without a leading edge Kruger flap (shown on the aircraft in Figure 1) and discussed in reference [3]. The tests were conducted with the aircraft hovering out of ground effect in winds less than 3 knots. Once steady hover was established, a baseline AFC-off data point was taken. The pilots then set the proper AFC frequency and amplitude on the MAFC Controller and engaged the system. The aircraft was trimmed once again to attain steady hover and a second AFC-on data point was taken. This procedure was repeated for six different RPM settings at each flap deflection, and for flap deflections ranging from 55 to 80 degrees.

During the flight tests, the pressure difference across the actuators and the actuator temperature were closely monitored. As shown in Figure 32, the actual pressure differentials were very close to those predicted from the full-scale flap wind tunnel tests described earlier. They were much higher than those seen in the U of A powered model tests, and we attribute this difference to the importance of scaling the details of the flap environment in such a pressure difference. The difficulty in replicating these details on the smaller model of the powered tests, including the gap arrangement between the main element and the flap, is the most likely reason for this difference. This crucial outcome of the model-flap tests in the NDF alone is sufficient to justify the effort involved in this second phase of testing. Because of this a priori knowledge, only two actuator failures occurred throughout the flight tests. These failures and their specific locations were immediately detected by the actuator health monitoring instrumentation. Both were determined to be mechanical failures, and actuator temperatures never approached the maximum safe operating temperature during the tests. Due to the design of the flaps and actuators, replacing failed actuators was quickly accomplished with the aircraft on

the flight ramp; it was not necessary to bring the aircraft into the hangar. Whenever an actuator was replaced, and at other times throughout the flight tests, the AFC system performance was checked using the total-pressure tube in the calibration fixture described in the previous section. This was done both on the flight ramp and in the hangar between flights. Examples of these checks are shown in Figure 33. The performance remained essentially unchanged throughout the flight tests.

6.2 Success Criteria

Based on the powered model tests, two success criteria were defined prior to the start of the flight tests. These are discussed in reference [3] and illustrated in Figure 34. Success Criterion 1 concerned the maximum download reduction due to AFC at a single flap deflection, one that is separated without AFC. The goal for this criterion was a download reduction of 14%, or about 220 lb (100 kg). Success Criterion 2 concerned the maximum performance benefit of AFC, measured as the reduction in download from the minimum baseline case to the minimum AFC-on case. The goal for this criterion was a 9% reduction in download, or about 150 lb (68 kg).

6.3 Results

Results of the flight tests were reported in references [2] and [3], and are shown again in Figures 35 and 36 of this paper. These figures show variations of rotor power coefficient with weight coefficient. The curves were constructed from the data taken at different RPM settings for a given flap deflection. Figure 35 shows the results applicable to Success Criterion 2. The AFC-off case is shown for a flap deflection of 70 degrees, which corresponds to the minimum download condition without AFC. The AFC-on case presented here is for a flap deflection of 75 degrees, which corresponds to the minimum download condition with AFC engaged. The AFC-on curve is below and to the right of the baseline curve, indicating that with AFC, more weight can be carried for a given power setting or less power is required for a given weight. The resulting download reduction is approximately 150 lb, or 9%, which met the goal of this aspect of the tests.

Figure 36 shows the results applicable to Success Criterion 2. Here, both curves are for a flap deflection of 75 degrees. Again, an improvement is seen with the AFC system engaged. In this case, the reduction in download translates to approximately 220 lb, or 14%, which again met the goal. There is a very interesting phenomenon shown in this figure that was noticed at times during the flight tests. When AFC-on points were followed by AFC-off points within a sufficiently short period of time, the AFC-off download was very close to the preceding AFC-on value. This indicates that the effects of AFC persist for a period of time after the AFC is turned off. This can be seen in Figure 36 by the open symbol data points. This behavior suggests that, for a range of flap deflections, the separation over the flap is somewhat bi-stable. The AFC causes it to switch to an attached state, and it remains in this state for some time after the excitation is removed. This has important implications for the development of a true production AFC system for aircraft of this type. It could mean substantial power savings by applying AFC for short duty cycles rather than continuously, as was done in the testing described in this paper.

6.4 Discussion of Results

Table 1 shows the AFC parameters used for both the 16% powered-model tests at the University of Arizona and the full-scale flight tests. It should be noted that a wide range of frequencies and amplitudes were used for the powered-model tests, but only two representative cases are shown here. These cases summarize what might be considered optimum or desirable operating conditions based on the model tests.

In the model tests, effective download reduction was achieved only after C_μ exceeded 0.5%. To match the C_μ of the 16% powered-model tests for the flight test, either the peak jet velocity (U_j) would have needed to be increased to 125 m/s or, the AFC slot width would have needed to increase to 6.35 mm while maintaining a peak jet velocity of 53 m/s. In the first case, the ratio U_j/U_∞ would have increased to 4.17, while in the second case this ratio would have decreased to 1.77.

Table 1: XV-15 16% Model Test and Flight Test AFC System Parameters

	h [mm]	**c** [m]	$\mathbf{x_{te}}$ [m]	**F** [Hz]	$\mathbf{U_\infty}$ [m/s]	$\mathbf{U_j}$ [m/s]	$\mathbf{C_\mu}$	$\mathbf{U_j / U_\infty}$	$\mathbf{F^+}$
16% Model Test	1.02	0.255	0.070	90	20.5	36.7	1.28%	1.79	0.62
16% Model Test	1.02	0.255	0.070	180	20.5	36.0	1.23%	1.75	0.31
Flight Test	1.14	1.592	0.442	50	30.0	61.9	0.31%	2.06	0.74
Flight Test	1.14	1.592	0.442	90	30.0	80.4	0.52%	2.68	1.18

With the current technology, neither of these two options were possible; but more importantly, they were not necessary to achieve the results shown in Figures 35 and 36. More importantly, the model tests with the full flap size in the NDF projected effective reduction of download for the parameters ultimately used in the flight tests. This indicates that successful AFC requires narrow jets with sufficient U_j/U_∞ ratios, of the order of 2 to 3, and that C_μ is not the proper AFC amplitude scaling parameter for large separated flow fields of this type. The results of these tests indicate that a broad range of F^+ values, possibly as low as 0.5 or smaller and as high as 2, leads to effective AFC. Other research has demonstrated that smaller separated regions, or ones that are highly receptive to large coherent structures, can be effectively and efficiently controlled using a more narrow range of F^+, around unity, with substantially lower values of C_μ ; about an order of magnitude less. In these cases, which could be termed “excitable AFC of separation”, C_μ is the appropriate scaling parameter.

Regarding Figure 36, in this experiment the flow was forcefully attached by the excitation when it was switched on by the pilots. Once the flow was attached and the excitation was switched off, it took time for the flow to re-separate. Therefore, there is a hysteresis between the application of control and the establishment of separation, not unlike what has been observed with dynamic stall, such as on helicopter rotors.

7.0 CONCLUSIONS

The effectiveness of periodic Active Flow Control (AFC) was successfully demonstrated, at both model scale and at full scale, in reducing the download on the wings of a hovering XV-15 aircraft. The following are the main results and conclusions.

- Scaled XV-15 powered-model tests with AFC applied at 10% flap chord showed that the download was reduced by 9% compared to the baseline value. With the addition of a passive leading edge Krueger flap, the download was reduced by 20% of the baseline value.

- Full-scale tests on the XV-15 aircraft without a Krueger flap showed that the download was reduced by 9%, in agreement with the scale model tests. Tests with a Krueger flap showed an 18% reduction in download closely comparable to the 20% reduction seen in the model.

- Tests on powered scaled tiltrotor models can be used effectively to model full-scale download aerodynamics.

- Utilizing two model sizes, with different aspects of the full scale aircraft represented in them, is a most effective way to reveal the degree of sensitivity to important physical phenomena such as the interaction between transition and separated regions, and to establish the appropriate AFC parameters for the full scale vehicle. It can also reduce the risks involved with the flight testing and improve the efficiency of the tests.

Under the recent MAFC program of DARPA, a great deal of accomplishment and maturation of Active Flow Control (AFC) was achieved, partly due to the results discussed here. We now recognize that not all separated flows are amenable to the same strategies for their effective control; e.g., small versus large separated regions and localized as contrasted to meandering initiation of the separation zone. A major obstacle in the way of achieving realistic flow control in flight has been the actuators. The present work contributed substantially to progress in this challenging area.

Pioneering efforts in AFC had exploited periodic excitation, and demonstrated great promise in open-loop experiments by completely altering the mean flow much more quickly than is possible using conventional ailerons or rudders. In this type of AFC, small input disturbances are naturally amplified by the flow external to the body. Thus, the considerable energy needed to cause a change in the steady-state behavior of the flow is extracted from the mean flow, and actuator power requirements are low. The research described here has utilized lower frequencies of excitation and higher velocities through narrower slots to achieve control of larger separations associated with large deflections of aerodynamic surfaces.

We can now conclude with some confidence that, wherever there is a separated flow of a fluid over a surface, AFC can reduce the separation and lower the system energy loss. This can often lead to increasing the maximum lift and reducing drag on wings, rotors, compressors, etc. It can also be utilized in thrust vectoring or to replace control surfaces; etc. We envision that in the near future, AFC will have a large range of potential applications to aircraft, ships, submarines, internal flow systems, combustors, and many other complex systems and devices.

8.0 ACKNOWLEDGEMENTS

This material is based upon work supported in part by the MAFC program of the U. S. Defense Advanced Research Projects Agency (DARPA) through contract number DAAD19-99-C-0023. The authors wish to acknowledge the assistance of Dr. Steve Walker, DARPA, and Mr. Matt Tallent, Centra Technology, Inc. during the execution of this work. The MAFC program of DARPA was initiated under the leadership of Dr. James McMichael and for several years was managed by Dr. Richard Wlezien, before Dr. Steve Walker took on the responsibility. Their vision and support of the program leading to these successful flight tests described here is also acknowledged.

9.0 REFERENCES

[1] A. Darabi, D. Cerchie, L. Cullen, A. Stalker, I. Wygnanski, M. A. McVeigh, "Download Alleviation for the XV-15: Exploration of Load Reduction Possibilities Using a 16% Airplane Model." AIAA International Powered Lift Conference, Williamsburg, VA, Nov. 2002.

[2] M. A. McVeigh, H. Nagib, T. Wood, J. Kiedaisch, A. Stalker, I. Wygnanski, "Model & Full Scale Tiltrotor Download Reduction Tests Using Active Flow Control." AHS 60th Annual Forum, Baltimore, MD, June 2004.

[3] A. Stalker, D. Cerchie, L. Cullen, I. Wygnanski, "Using Periodic Perturbations for Download Alleviation on Tilt-Rotor Airplane Models in Hover." AIAA Paper 2004-2515, 2nd AIAA Flow Control Conference, Portland, OR, June 2004.

[4] P. Kjellgren, N. Anderberg, I. Wygnanski, "Download Alleviation by Periodic Excitation on a Typical Tilt-Rotor Configuration – Computation and Experiment." AIAA Paper 2000-2697, AIAA Flow 2000, Denver, CO, June 2000.

[5] P. Kjellgren, D. Cerchie, L. Cullen, I. Wygnanski, "Active Flow Control on Bluff Bodies with Distinct Separation Locations." AIAA Paper 2002-3069, 1st AIAA Flow Control Conference, St. Louis, MO, June 2002.

[6] P. Kjellgren, A. Hassan, J Sivasubramanian, L. Cullen, D. Cerchie, I. Wygnanski, "Download Alleviation for the XV-15: Computations and Experiments of Flows around the Wing." AIAA Paper 2002-6007, 2002 Biennial International Powered Lift Conference, Williamsburg, VA, November 2002.

Figure 1: Bell XV-15 Tiltrotor.

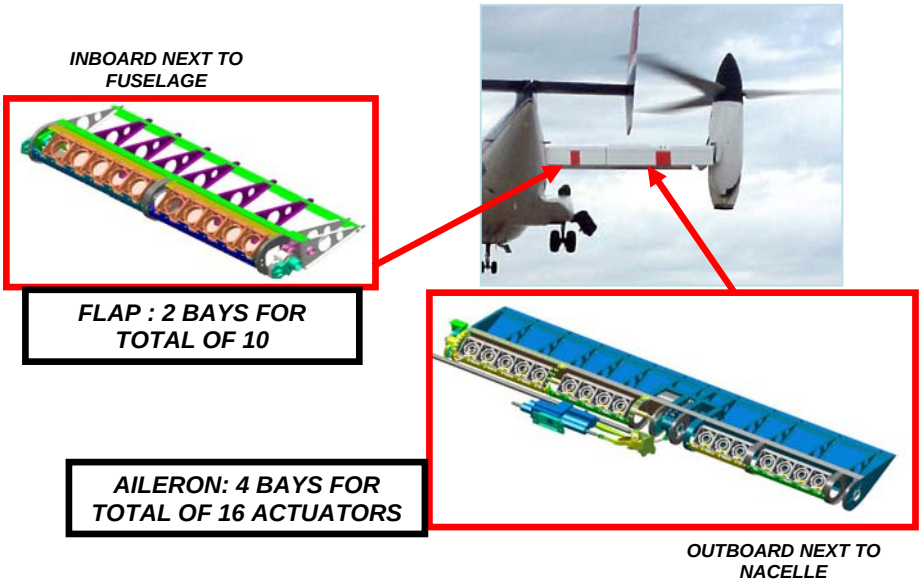

Figure 2: XV-15 AFC Flap Design.

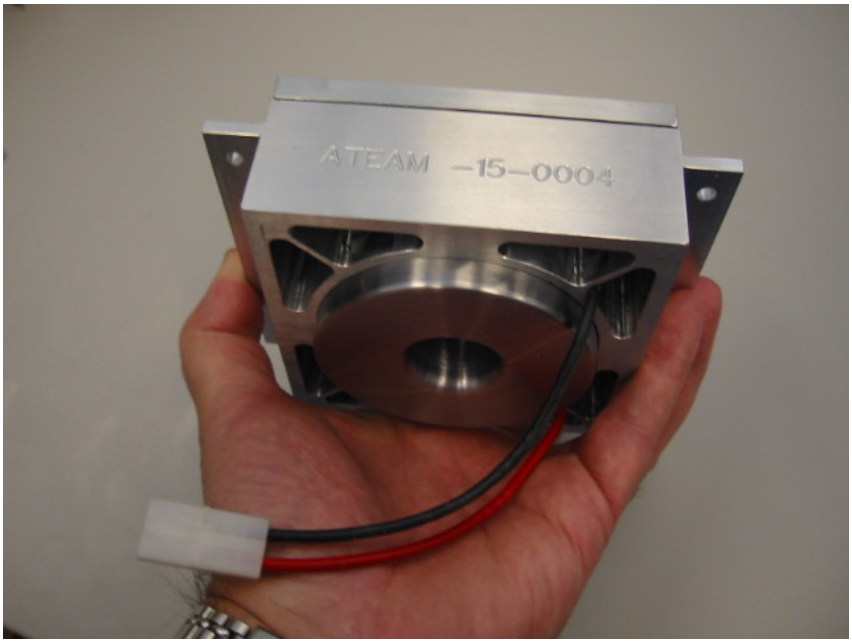

Figure 3: ATEAM-15 Actuator used for XV-15 Flight Tests.

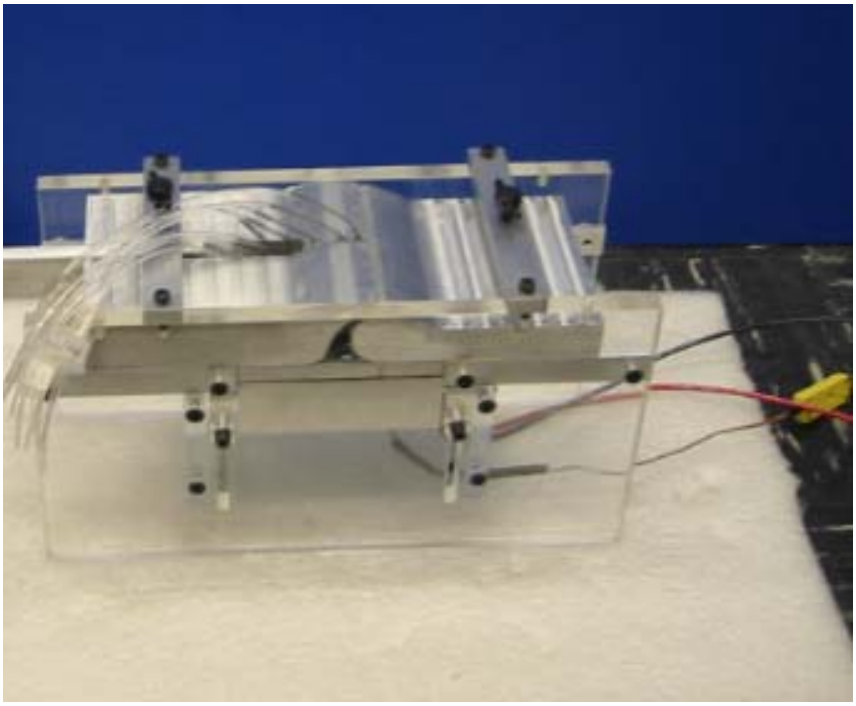

Figure 4: Single Actuator and Slot Test Fixture.

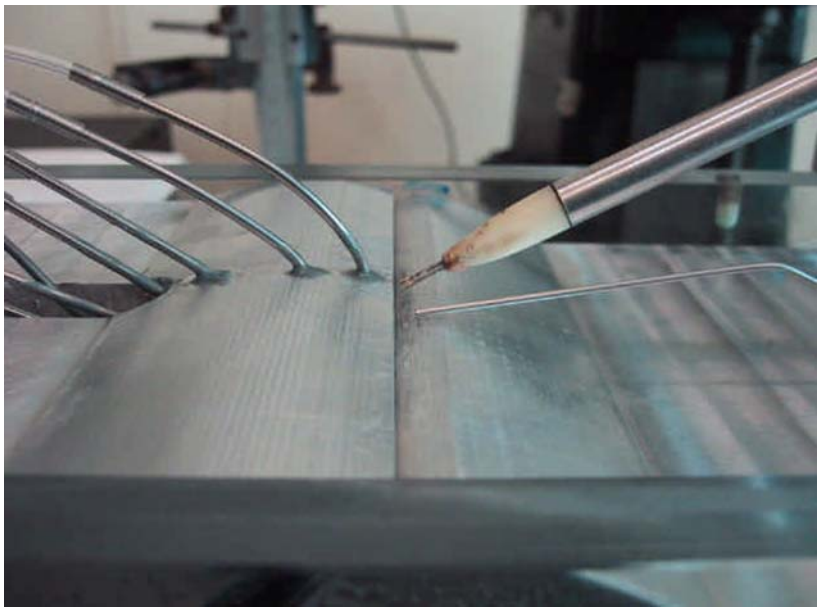

Figure 5: Calibration Using Hot-wire and Pitot Tube.

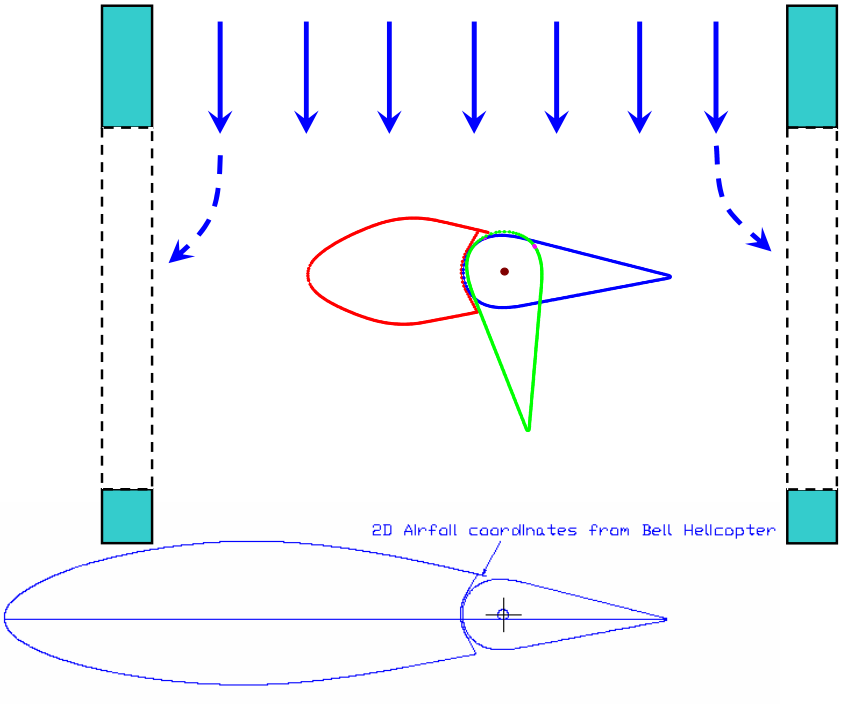

Figure 6: Full-Scale Flap Model Concept.

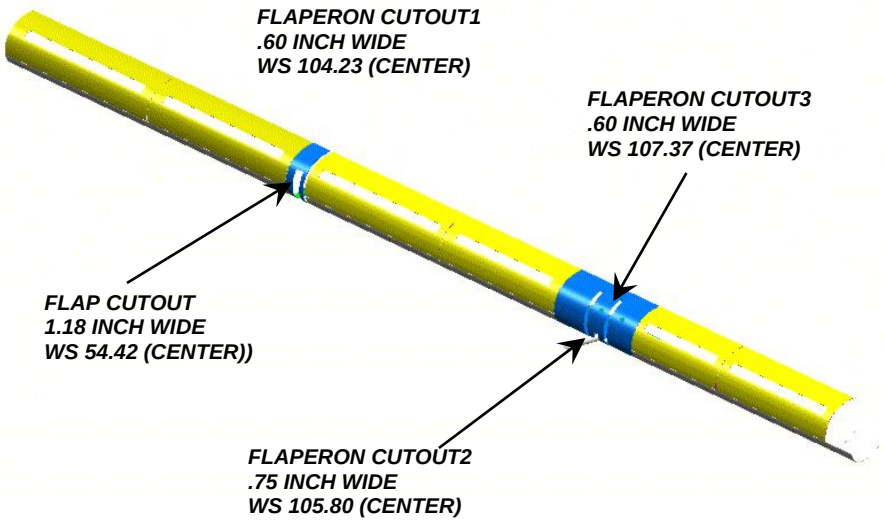

Figure 7: XV-15 Flap Leading Edge Details.

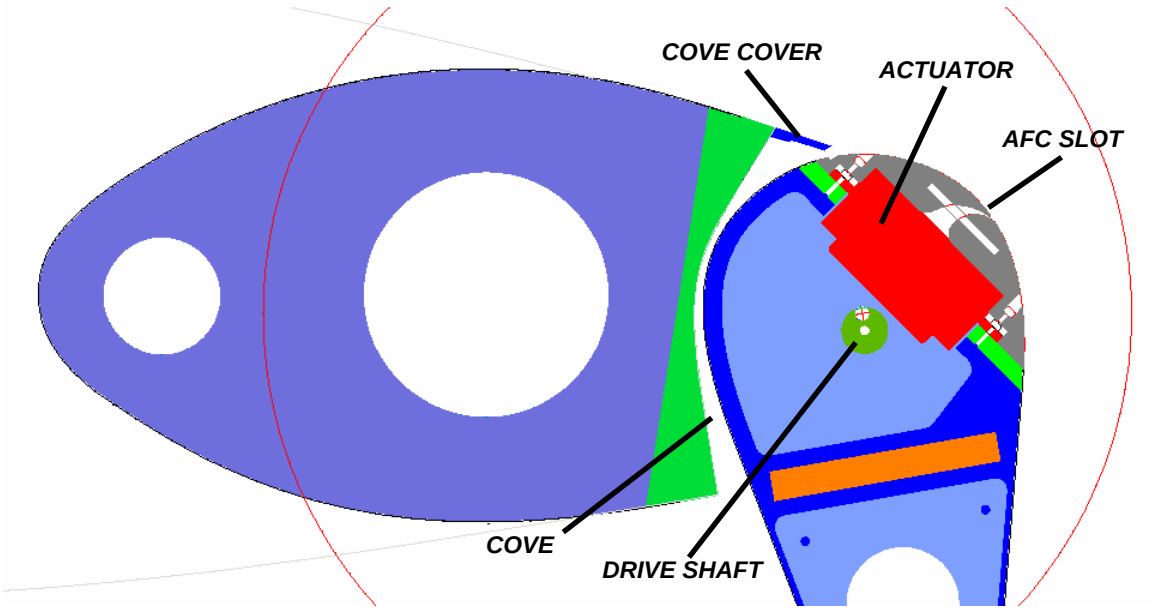

Figure 8: Full-Scale Flap Model design Details.

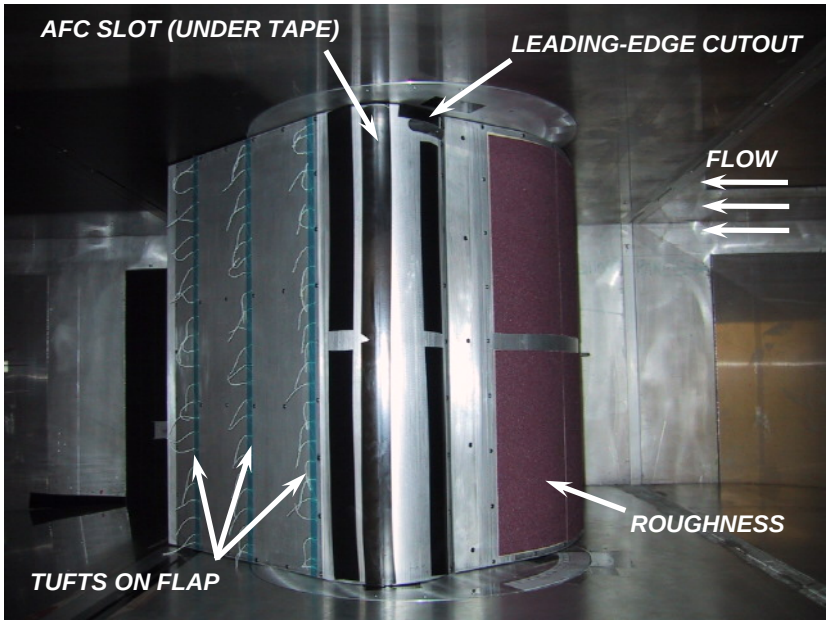

Figure 9: Full-Scale Flap Model Installed in NDF Test Section.

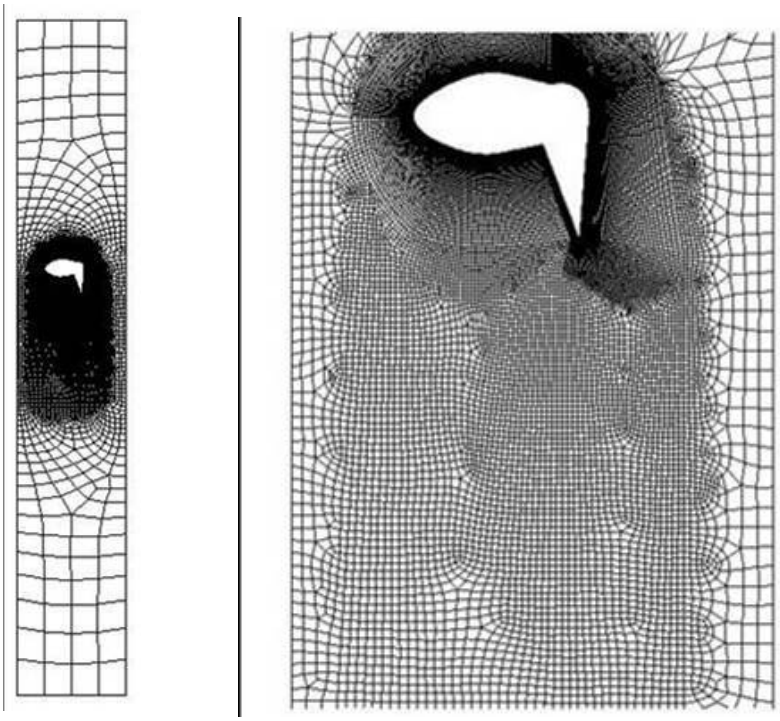

Figure 10: Grid for CFD Analysis.

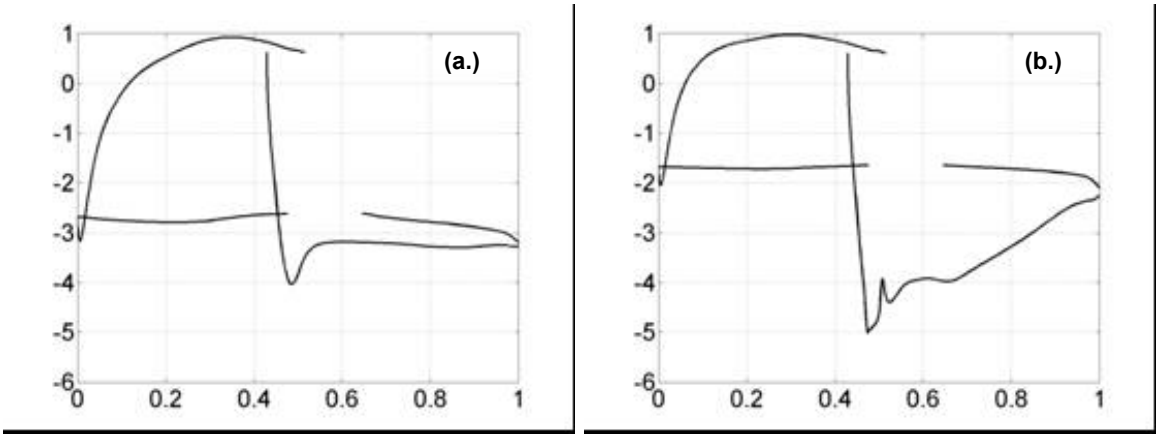

Figure 11: Full-Scale Flap Model CFD Results - c_p Distributions; (a.) Baseline, (b.) Forcing @ Cμ=1.5%, F+=0.33.

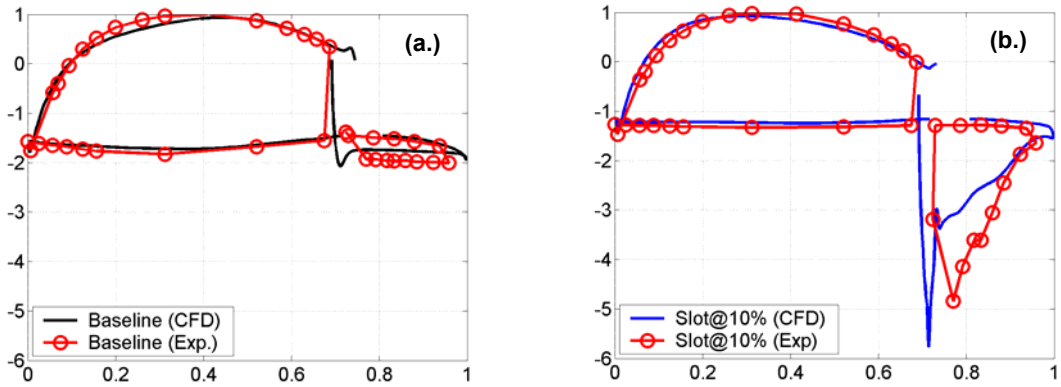

Figure 12: XV-15 Wing CFD and Experimental Results – c_p Distributions, α=-85, δ_f=80; (a.) Baseline, (b.) Forcing @ Cμ=1.5%, F+~1.

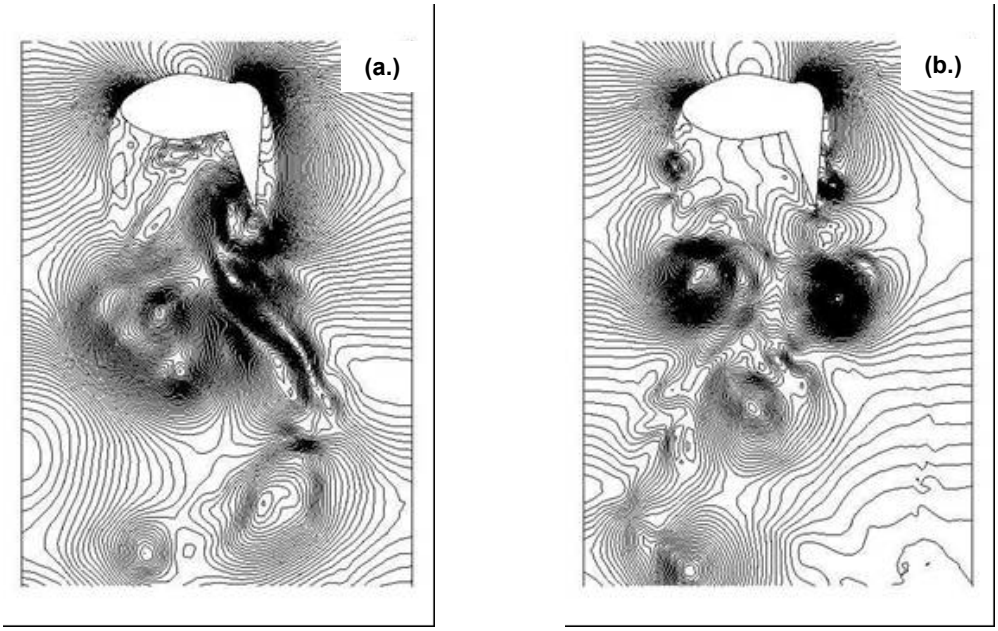

Figure 13: Full-Scale Flap CFD Results – Instantaneous Pressure Contours; (a.) Baseline, (b.) Forcing @ Cμ=1.5%, F+=0.33.

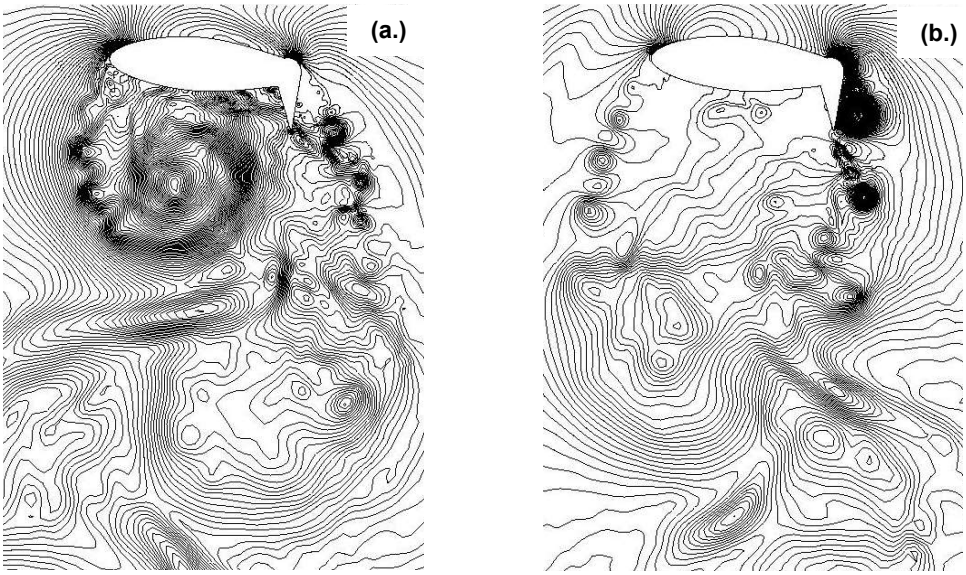

Figure 14: XV-15 Wing CFD Results – Instantaneous Pressure Contours, α=-85, δ_f=80; (a.) Baseline, (b.) Forcing @ Cμ=1.5%, F+~1.

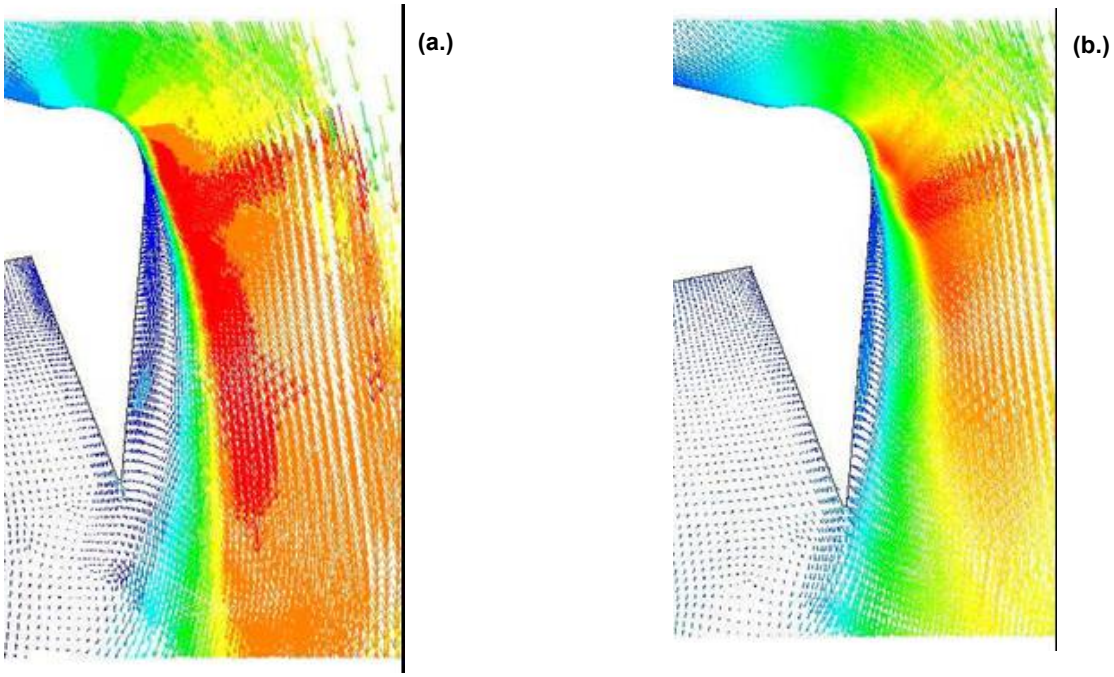

Figure 15: Time-Averaged Velocity Vectors; (a.) Baseline, (b.) Forcing @ Cμ=1.5%, F+=0.33.

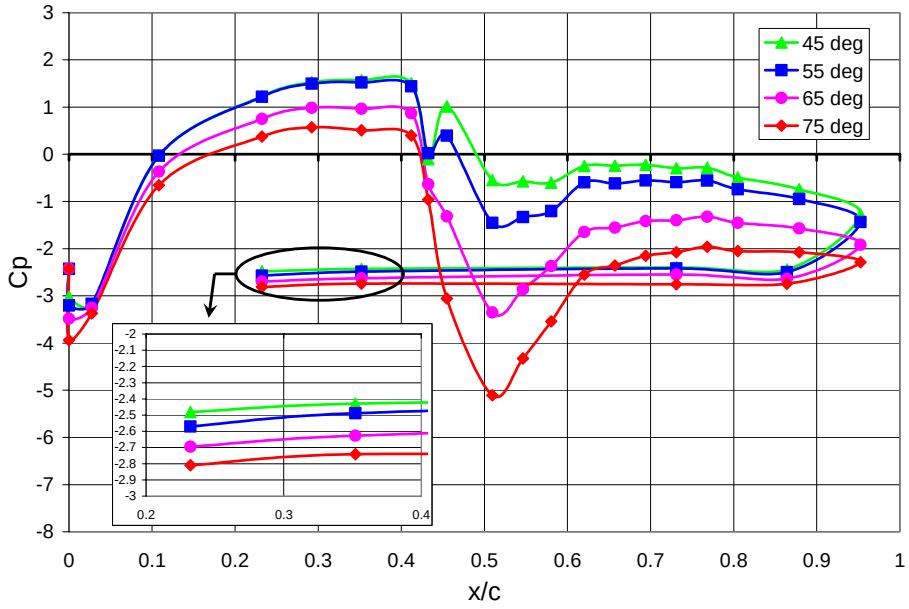

Figure 16: c_p Distribution for α=-90 deg. (with Added Roughness).

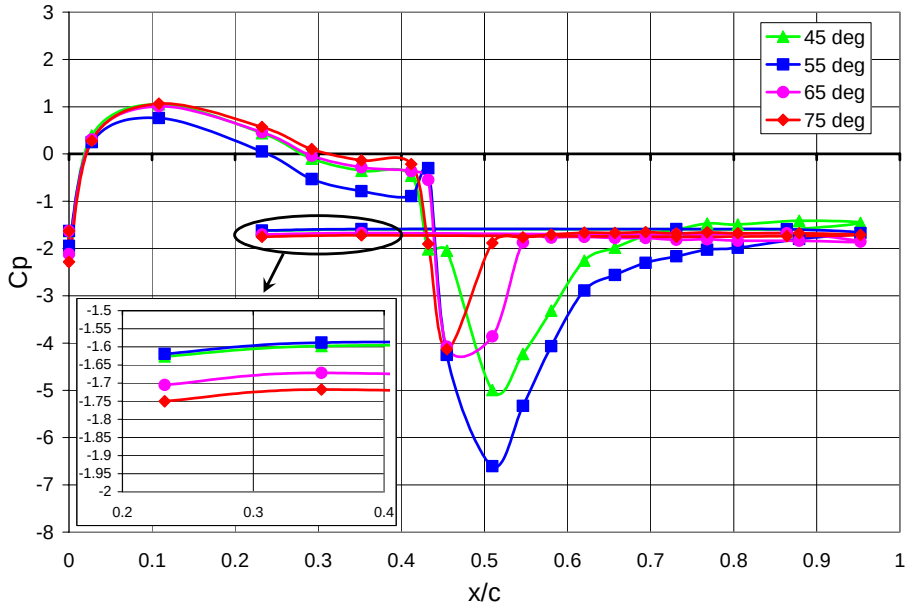

Figure 17: c_p Distribution for α=-50 deg. (with Added Roughness).

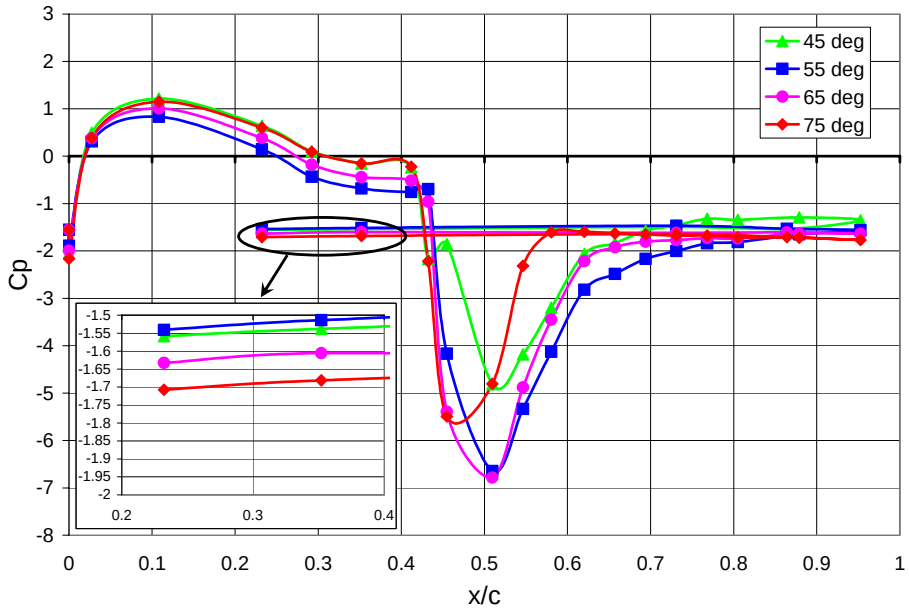

Figure 18: c_p Distribution for α=-50 deg. (without Added Roughness).

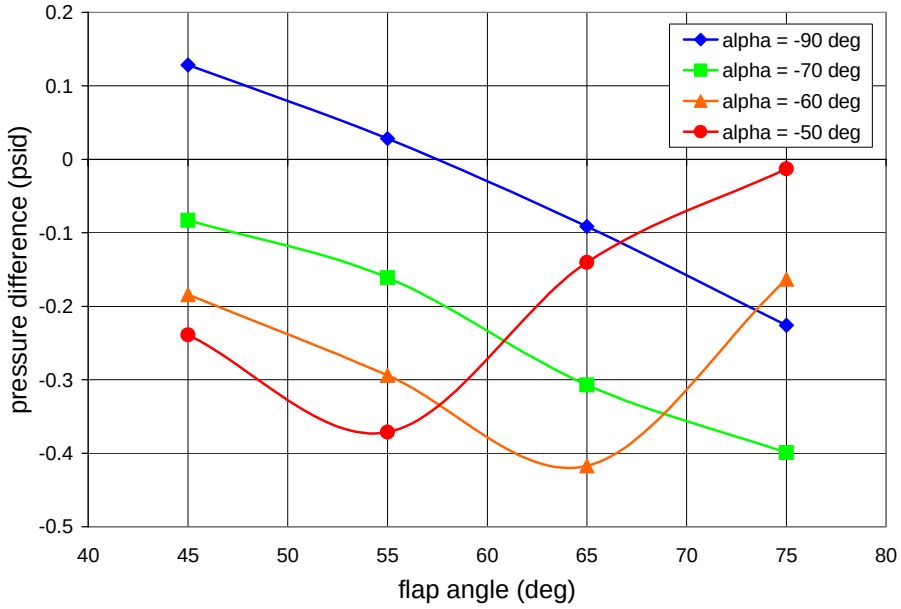

Figure 19: Pressure Difference Across Actuators for U_∞=30 m/s.

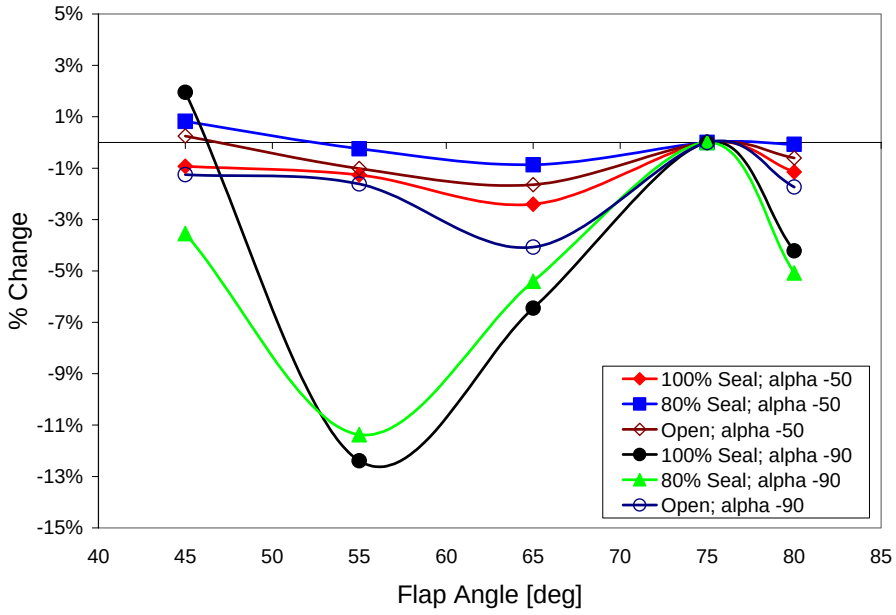

Figure 20: Effect of Sealing Cove on Flap Model Base Pressure.

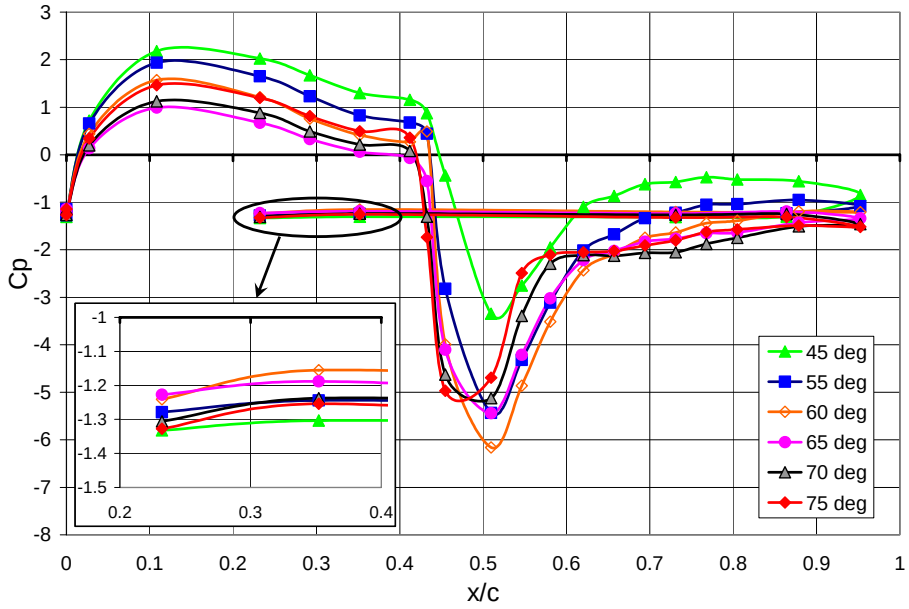

Figure 21: c_p Distributions for α=-60 deg. and Sealed Cove.

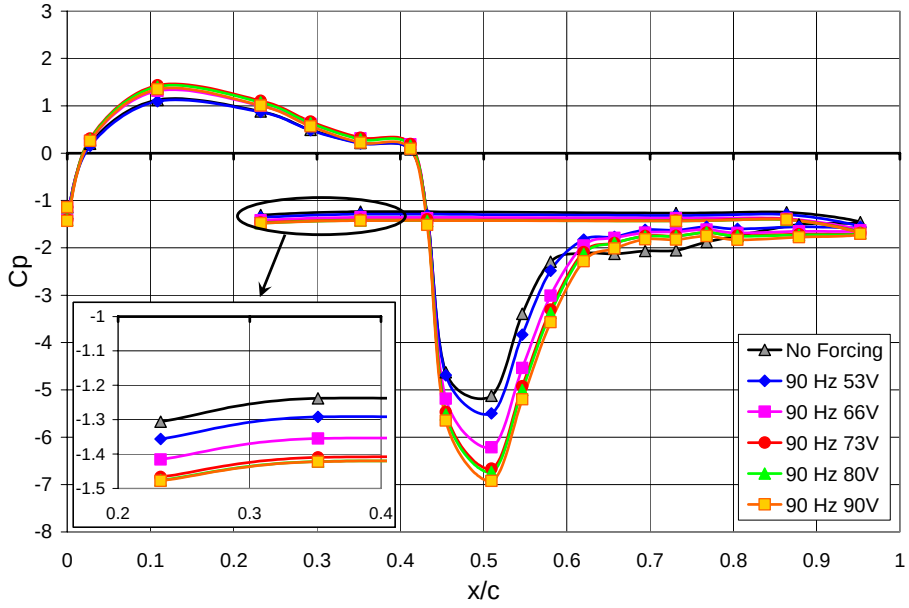

Figure 22: c_p Distributions, Baseline and with AFC, for α=-60 deg. δ_f=70 deg. and Sealed Cove.

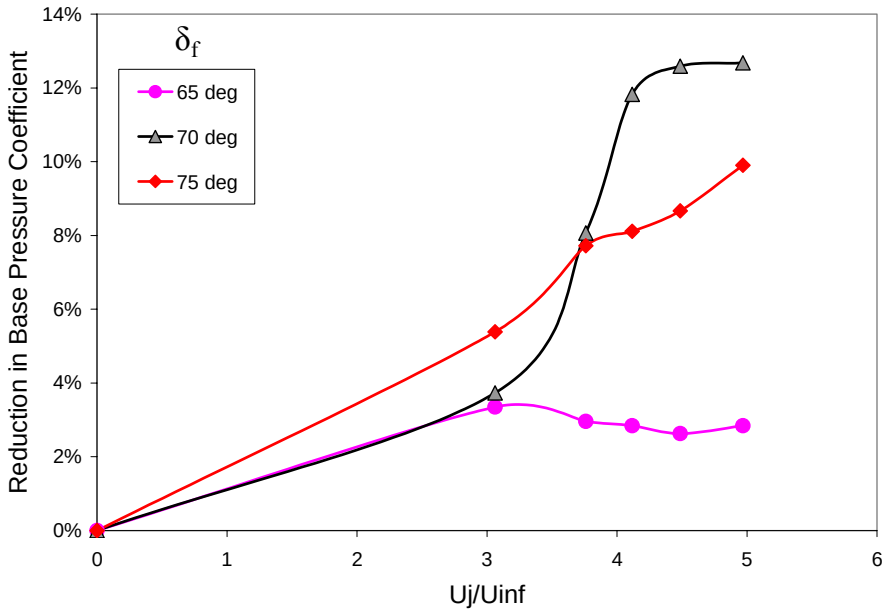

Figure 23: Reduction in Base Pressure Coefficient with Increasing AFC Amplitude for α=-60°.

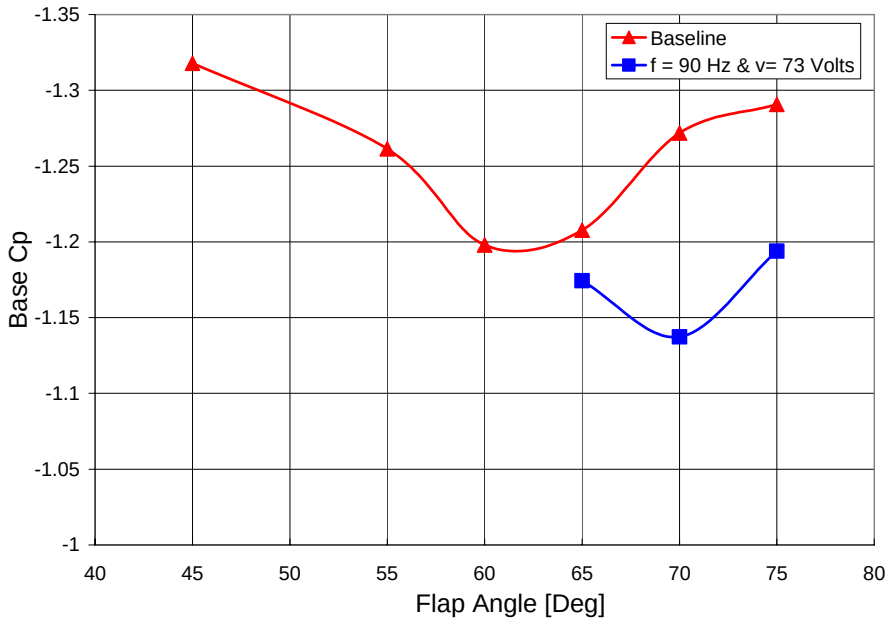

Figure 24: Base Pressure at Different Flap Deflections, Baseline and AFC, α=-60°.

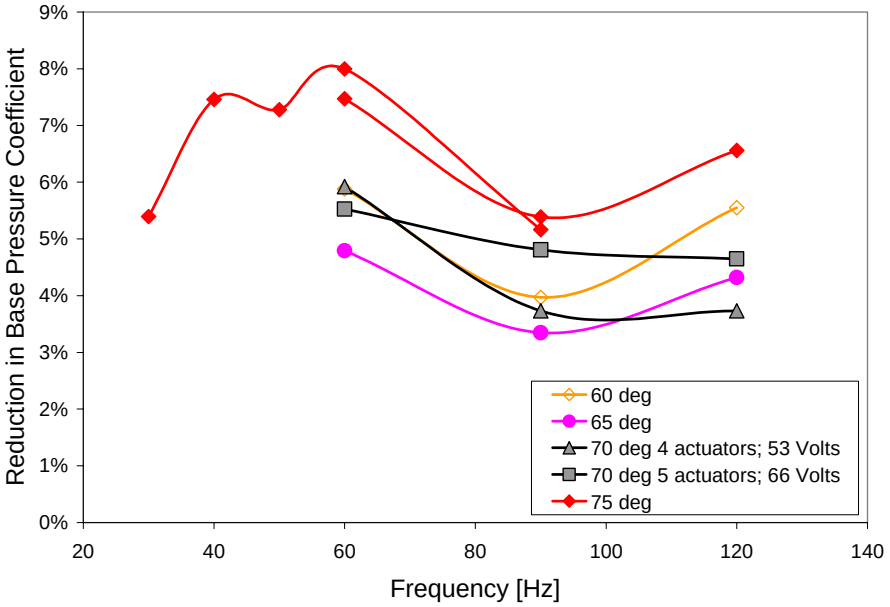

Figure 25: Reduction in Base Pressure Coefficient with AFC for Different Forcing Frequencies.

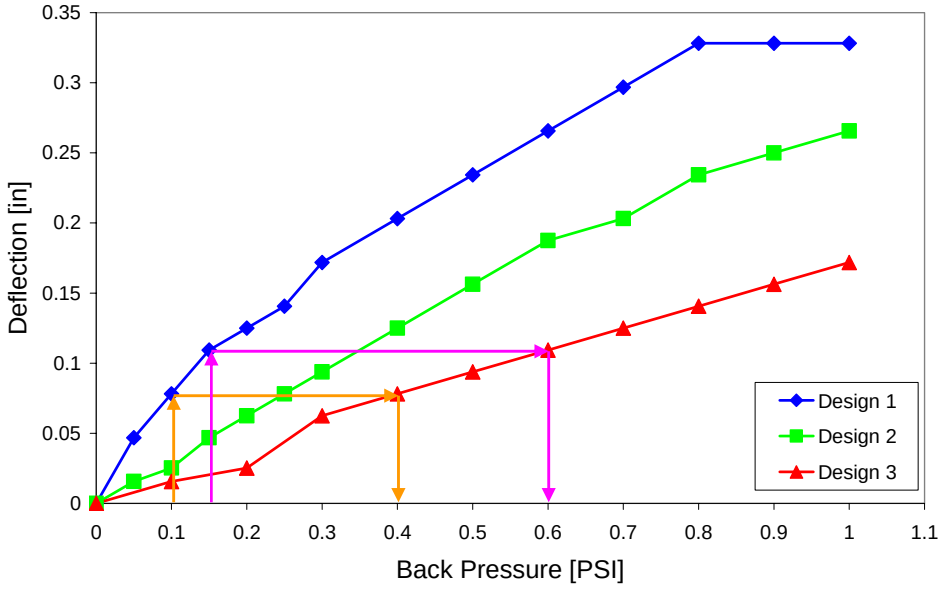

Figure 26: ATEAM-15 Actuator Piston Deflection for Different Back Pressures.

Figure 27: ATEAM-15 Actuators Installed in the XV-15 Flap.

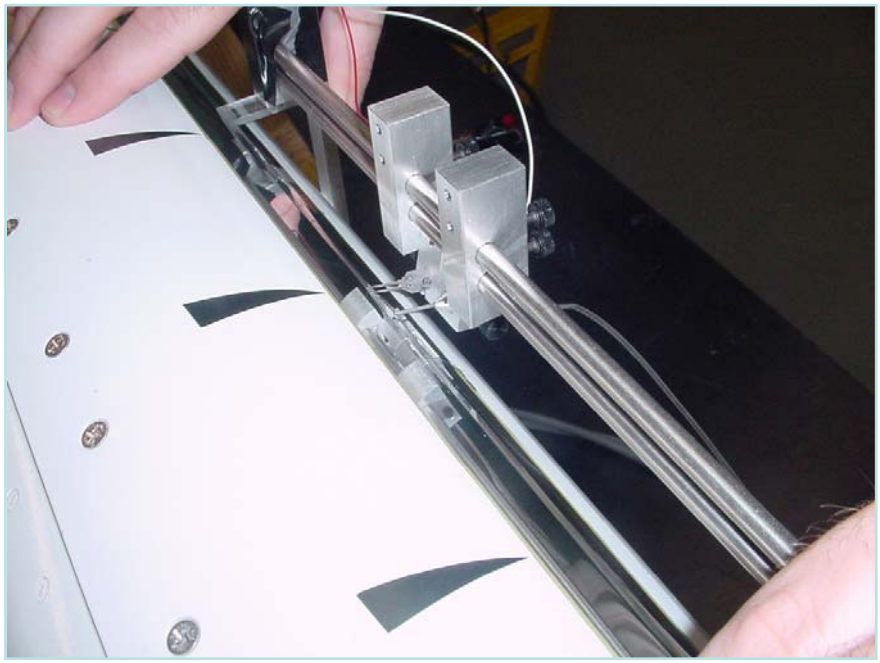

Figure 28: Hot-wire and Total-Pressure Calibration Fixture Positioned at Slot Exit on XV-15 Flap.

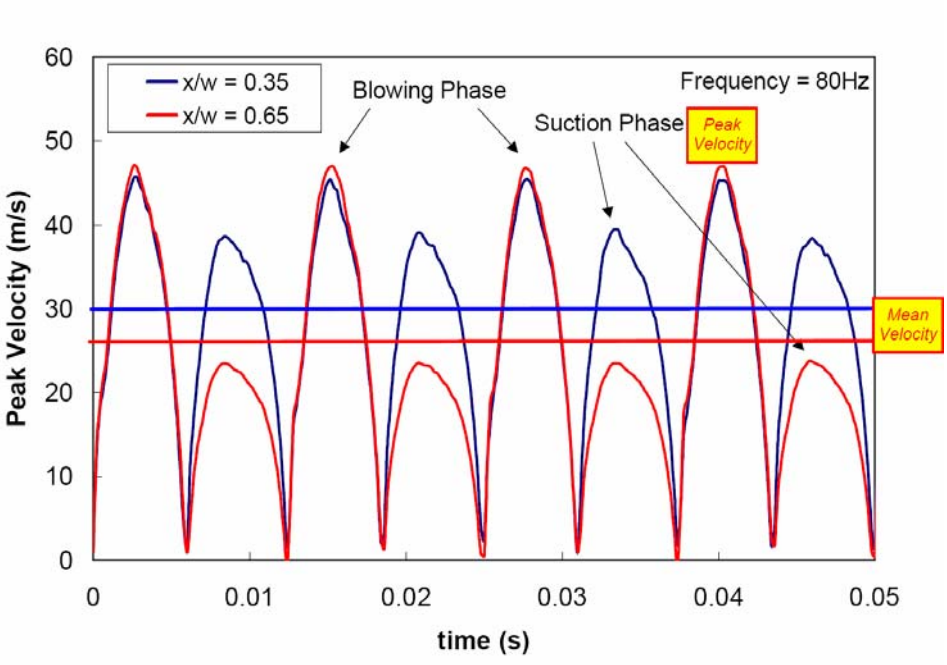

Figure 29: Hot-wire Calibrations of AFC Slot Velocity.

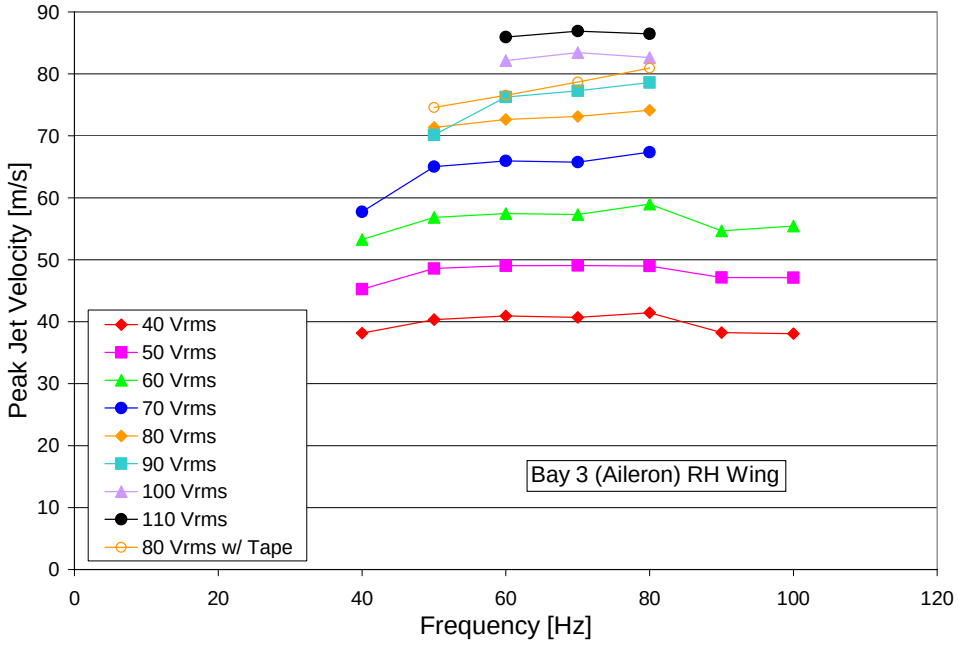

Figure 30: Sample Calibration of XV-15 Flap AFC Performance.

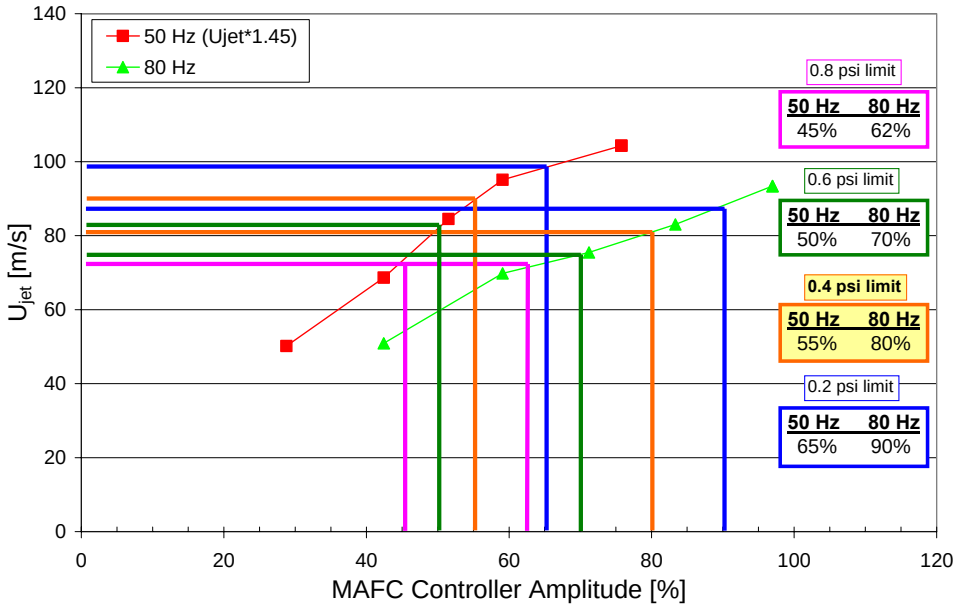

Figure 31: XV-15 AFC System Operating Envelope.

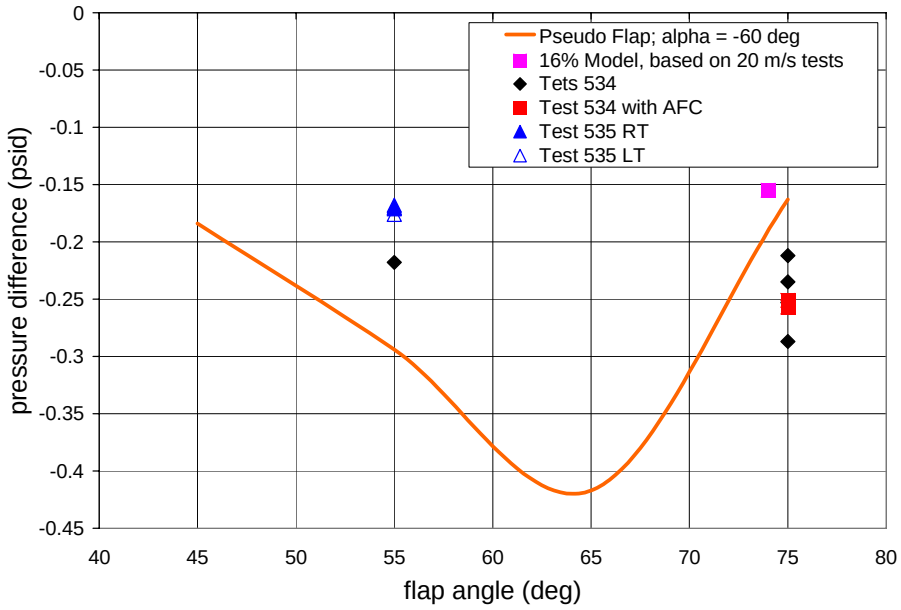

Figure 32: Comparison of Experimental and Actual Pressure Difference Across Actuators.

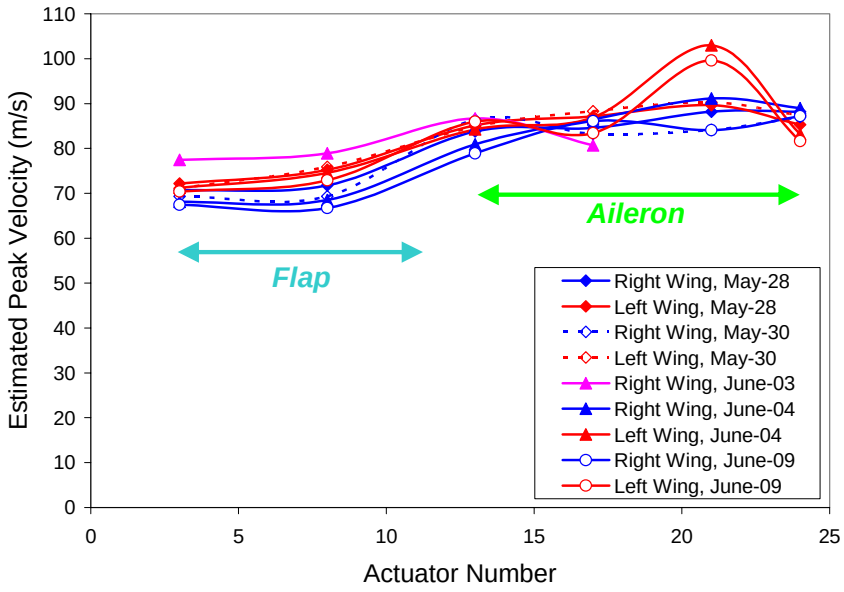

Figure 33: Calibrations of XV-15 AFC System Performance at Various Points During Flight Tests.

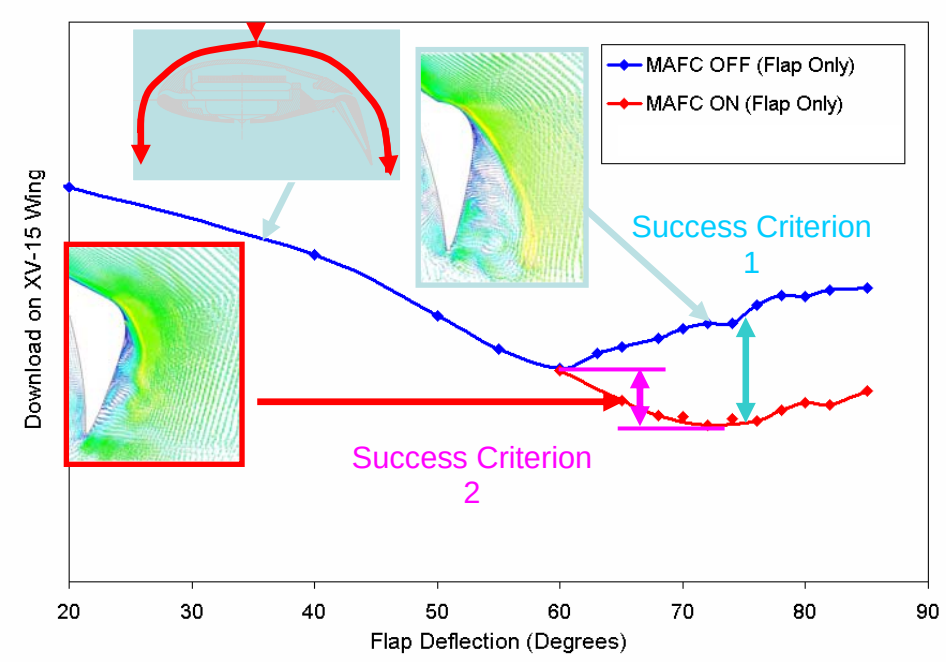

Figure 34: Definition of XV-15 Flight Test Success Criteria.

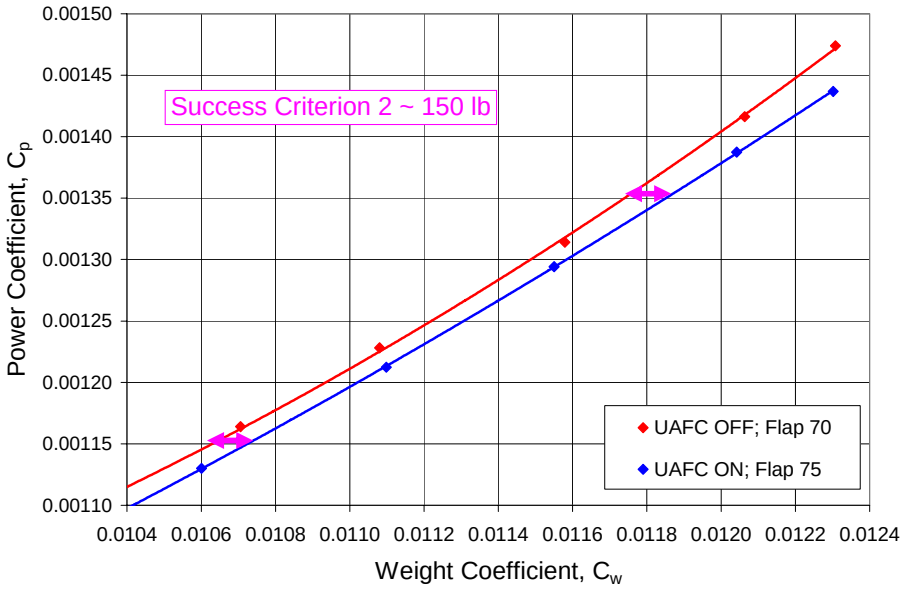

Figure 35: XV-15 Flight Test Results; AFC Performance for Success Criterion 2.

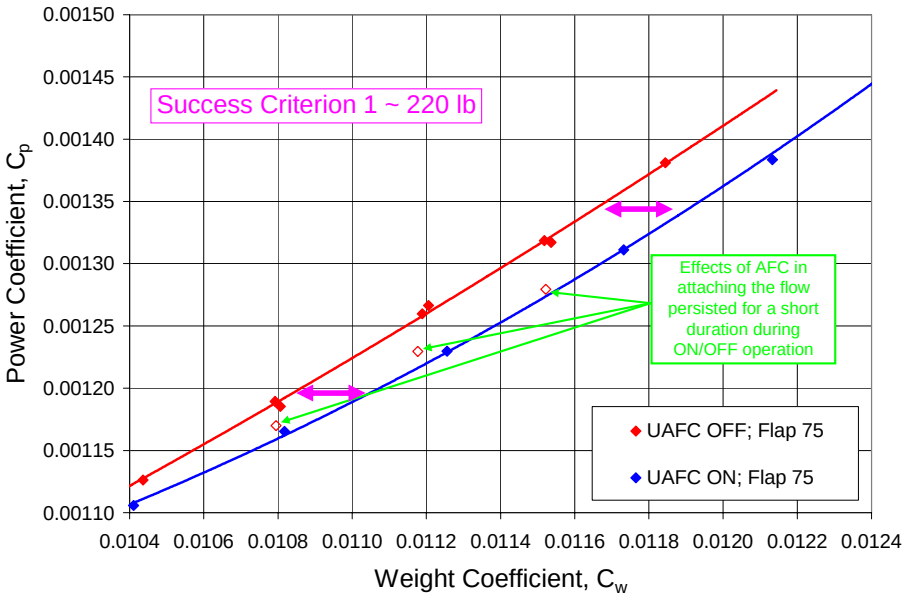

Figure 36: XV-15 Flight Test Results; AFC Performance for Success Criterion 1.